

Microscopic Coexistence of Magnetism and Superconductivity in charge compensated $\text{Ba}_{1-x}\text{K}_x(\text{Fe}_{1-y}\text{Co}_y)_2\text{As}_2$

Til Goltz,¹ Veronika Zinth,² Dirk Johrendt,² Helge Rosner,³ Gwendolyne Pascua,⁴ Hubertus Luetkens,⁴ Philipp Materne,¹ and Hans-Henning Klauss¹

¹*Institute of Solid State Physics, TU Dresden, D-01069 Dresden, Germany*

²*Department Chemie der Ludwig-Maximilians-Universität München, D-81377 München, Germany*

³*Max Planck Institute for Chemical Physics of Solids, D-01187 Dresden, Germany*

⁴*Laboratory for Muon-Spin Spectroscopy, Paul Scherrer Institut, CH-5232 Villigen PSI, Switzerland*

(Dated: February 5, 2014)

We present a detailed investigation of the electronic phase diagram of effectively charge compensated $\text{Ba}_{1-x}\text{K}_x(\text{Fe}_{1-y}\text{Co}_y)_2\text{As}_2$ with $x/2 \approx y$. Our experimental study by means of x-ray diffraction, Mössbauer spectroscopy, muon spin relaxation and ac susceptibility measurements on polycrystalline samples is complemented by density functional electronic structure calculations. For low substitution levels of $x/2 \approx y \leq 0.13$, the system displays an orthorhombically distorted and antiferromagnetically ordered ground state. The low temperature structural and magnetic order parameters are successively reduced with increasing substitution level. We observe a linear relationship between the structural and the magnetic order parameter as a function of temperature and substitution level for $x/2 \approx y \leq 0.13$. At intermediate substitution levels in the range between 0.13 and 0.19, we find superconductivity with a maximum T_c of 15 K coexisting with static magnetic order on a microscopic length scale. For higher substitution levels $x/2 \approx y \geq 0.25$ a tetragonal non-magnetic ground state is observed. Our DFT calculations yield a significant reduction of the Fe 3d density of states at the Fermi energy and a strong suppression of the ordered magnetic moment in excellent agreement with experimental results. The appearance of superconductivity within the antiferromagnetic state can be explained by the introduction of disorder due to non-magnetic impurities to a system with a constant charge carrier density.

PACS numbers: 74.70.Xa, 74.25.Dw, 74.62.Dh, 76.80.+y, 76.75.+i,

I. INTRODUCTION

Shortly after the discovery of superconductivity in the electron-doped 1111 ferropnictides,¹ the structural related AFe_2As_2 -based compounds ($\text{A}=\text{Ba}$, Sr and Ca) were also found to display superconductivity when magnetic order is sufficiently suppressed by chemical substitution or applying pressure.²⁻⁷

Changing the nominal electron count e by introducing transition metal (TM) dopants on the Fe site or replacing the alkaline earth by an alkaline metal on the Ba site in BaFe_2As_2 is one strategy. Electron doping on the Fe site using $\text{TM} = \text{Co}$, Ni , Rh , Pd , Ir and Pt in $\text{Ba}(\text{Fe}_{1-x}\text{TM}_x)_2\text{As}_2$ leads to superconductivity and coincident phase diagrams for the 3d and 4d elements were found after appropriate scaling of x and e .⁸⁻¹² This includes the suppression of the structural (tetragonal-to-orthorhombic) and the antiferromagnetic (AFM) phase transition temperatures (T_S , T_N) and the appearance of a superconducting dome. Hole doping on the Ba site by substitution with K likewise introduces superconductivity¹³ and the obtained T - e phase diagrams for $\text{Ba}_{1-x}\text{K}_x\text{Fe}_2\text{As}_2$ and $\text{Ba}(\text{Fe}_{1-x}\text{Co}_x)_2\text{As}_2$ show similar properties: T_S and T_N are suppressed with increasing substitution and superconductivity appears once the AFM order is sufficiently weakened. In addition, there is conclusive evidence for microscopic coexistence of magnetism and superconductivity prior to the full suppression of the magnetic order in both systems.^{14,15} In

contrast to hole doping on the Ba site, in-plane substitution of Fe by Mn^{16} and Cr^{17} does not introduce superconductivity. Also, electron doping with Cu does not support superconductivity⁷ except below 2 K in the vicinity of $x_{\text{Cu}} \approx 0.044$.¹⁰ However, the precise role that each substituent plays in controlling magnetism and/or the appearance of superconductivity is still under debate. In particular, the effect of impurity scattering, disorder and their impact on the electronic structure or the dichotomy between localized and itinerant physics are still matters of discussion.^{10,18-21}

The study of systems with nominal isovalency as realized in the quaternary systems $\text{Ba}(\text{Fe}_{1-x}\text{Ru}_x)_2\text{As}_2$ ²² and $\text{BaFe}_2(\text{As}_{1-x}\text{P}_x)_2$ ²³ is thus straightforward to get a better understanding of this issue. Even without carrier doping, both systems display superconductivity albeit much higher substitution levels of $x_{\text{Ru}} \geq 0.18$ and $x_{\text{P}} \geq 0.2$ are needed to sufficiently suppress T_N and T_S . Notably, the case of Ru substitution is suitable for a comparison to transition metal substitution since the only modifications within the FeAs plane are done on the same site. A similar approach in which the in-plane modifications are limited to the substitution on the Fe site while maintaining nominal isovalency was proposed by Suzuki et. al.:²⁴ They report superconductivity by combining Co and K substitution in the quaternary system $\text{Ba}_{1-x}\text{K}_x(\text{Fe}_{1-y}\text{Co}_y)_2\text{As}_2$ with $x/2 \approx y = 0.14 - 0.22$. In the context of studying the influence of increasing in-plane substitution level on structure, mag-

netism and superconductivity, the charge compensated $\text{Ba}_{1-x}\text{K}_x(\text{Fe}_{1-y}\text{Co}_y)_2\text{As}_2$ system is of particular interest, since the Co states strongly resemble the Fe 3d states and the impurity potential of Co ($U_{\text{eff}} = 1.8 \pm 0.6$ eV) and Fe ($U_{\text{eff}} = 1.4 \pm 0.6$ eV) is rather similar.²¹

We synthesized and studied a series of polycrystalline samples of charge compensated $\text{Ba}_{1-x}\text{K}_x(\text{Fe}_{1-y}\text{Co}_y)_2\text{As}_2$ with a substitution level $x/2 \approx y$ ranging from 0 to 0.25. We complement our experimental results with a set of density functional theory calculations aiming to separate the effects of the crystallographic changes and the influence of double substitution onto the electronic structure. This investigation of the electronic phase diagram also continues earlier work on the solid solution $\text{Ba}_{1-z}\text{K}_z\text{Fe}_{1.86}\text{Co}_{0.14}\text{As}_2$, where we have shown, that a combination of Co and K substitution leads to an effective compensation of hole and electron doping near nominal charge compensation $z = 0.14$.²⁵ This result is in good agreement with photoemission data, showing a rigid-band-like filling or depleting of the electronic states near the Fermi level.²⁶ The result, that electron (hole) Fermi surface volumes increases (decreases) with substitution, is qualitatively consistent with a rigid-band model for TM=Co.²⁰ We conclude as a basic premise for this work, that for nominal charge compensated $\text{Ba}_{1-x}\text{K}_x(\text{Fe}_{1-y}\text{Co}_y)_2\text{As}_2$, the concept of isovalency due to effective electron and hole compensation is valid.

II. METHODS

Polycrystalline samples were prepared from stoichiometric mixtures of Ba, K and $(\text{Fe}_{1-y}\text{Co}_y)_2\text{As}_2$ in alumina crucibles, sealed in silica tubes and heated to 913 K. The samples were annealed at 983 K for 10 h, homogenized to a fine powder and annealed at 1063 K two times for 10 h. The Ba:K ratio was determined by the Rietveld analysis yielding an uncertainty for $x/2 \approx y$ of ± 0.02 . Details of the synthesis method are described in Ref.²⁵ Powder diffraction data were collected on a Huber G670 diffractometer with $\text{Co-K}\alpha_1$ or $\text{Cu-K}\alpha_1$ -radiation, equipped with a closed cycle He cryostat. From the AC susceptibility measurements, the superconducting transition temperature was extracted by fitting the steepest descent with a line and using the point of intersection with the normal-state susceptibility as T_c (onset). Mössbauer spectra were recorded in a standard transmission geometry setup using a $^{57}\text{Co}/\text{Rh}$ source with an emission line width (FWHM) of $\Gamma = 0.27(1)$ mm/s. The spectrometer was calibrated to $\alpha\text{-Fe}$ at room temperature. The powdered sample was mixed with methanol in a thin PA6.6 container to ensure a homogeneous surface thickness of 5 to 8 mg Fe/cm². A CryoVac Konti IT cryostat with He exchange gas was used to stabilize temperatures between 4.2 K and 300 K. Muon spin relaxation measurements were performed using the GPS spectrometer at the πM3 beamline of the Swiss Muon Source at the Paul

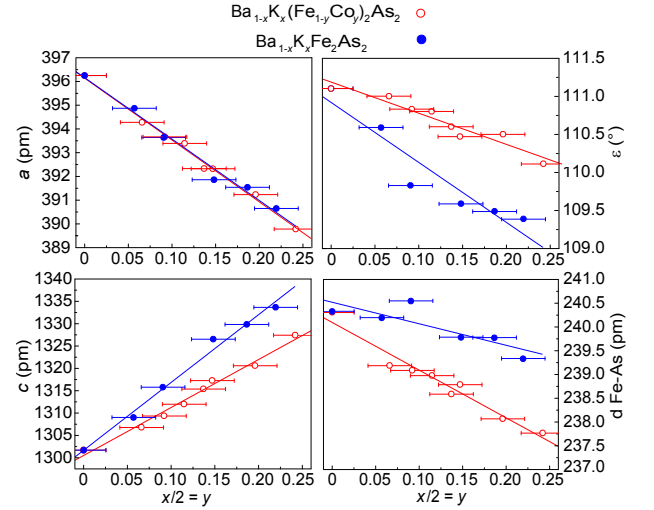


FIG. 1: Structural changes in charge compensated $\text{Ba}_{1-x}\text{K}_x(\text{Fe}_{1-y}\text{Co}_y)_2\text{As}_2$ (red, unfilled symbols) compared to $\text{Ba}_{1-x}\text{K}_x\text{Fe}_2\text{As}_2$ (blue, filled symbols) with increasing potassium content per FeAs-layer ($x/2$). Lattice parameter a (top left) and c (bottom left), As-Fe-As angle ε (top right) and Fe-As distance d (bottom right). Data for $\text{Ba}_{1-x}\text{K}_x\text{Fe}_2\text{As}_2$ is taken from Ref.¹³

Scherrer Institut, Switzerland. The data was analyzed with the MUSRFIT package.²⁷ Scalar-relativistic density functional (DFT) electronic structure calculations were performed using the full-potential FPLO code,^{28,29} version fplo9.01-35.⁸³ For the exchange-correlation potential within the local density approximation (LDA) the parametrizations of Perdew-Wang³⁰ was chosen. The calculations were carried out on a well converged mesh of 1728 k-points in the Brillouin zone (12x12x12 mesh) to ensure a high accuracy for details in the electronic density. The partial Ba substitution with K and Fe with Co, respectively, was modeled within the virtual crystal approximation (VCA).³¹ For each substitution, the calculations were carried out for the experimental lattice parameters³² if available, otherwise the structural data were linearly interpolated between neighboring experimental data points (see Fig. 1). For the simulation of the stripe antiferromagnetic order a $\sqrt{2} \times \sqrt{2}$ supercell within the tetragonal plane was chosen. The As- z position was optimized with respect to the total energy.

III. RESULTS

A. Structure

In Fig. 1, we show the structural parameters of charge compensated $\text{Ba}_{1-x}\text{K}_x(\text{Fe}_{1-y}\text{Co}_y)_2\text{As}_2$ (red) at room temperature compared to hole doped $\text{Ba}_{1-x}\text{K}_x\text{Fe}_2\text{As}_2$ ¹³ (blue) to emphasise the changes due to the additional in-plane Co substitution. While a is not affected by the additional cobalt substitution and decreases at the

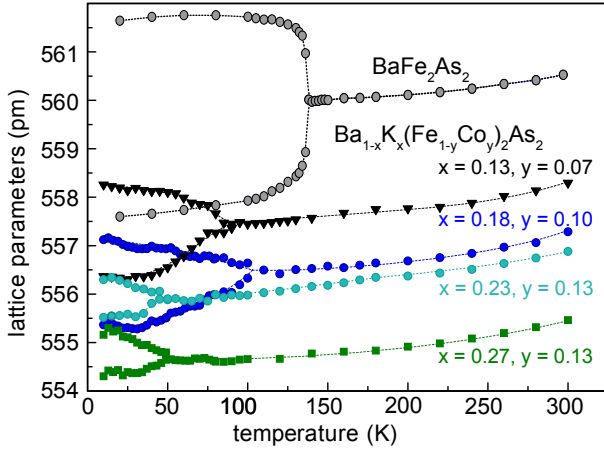


FIG. 2: Lattice parameters of $\text{Ba}_{1-x}\text{K}_x(\text{Fe}_{1-y}\text{Co}_y)_2\text{As}_2$ with $x/2 \approx y = 0.00 - 0.13$ (in orthorhombic notation), showing the orthorhombic splitting at low temperatures. Data for BaFe_2As_2 is taken from Ref.³³

same rate as in $\text{Ba}_{1-x}\text{K}_x\text{Fe}_2\text{As}_2$, the increase of c is clearly reduced in $\text{Ba}_{1-x}\text{K}_x(\text{Fe}_{1-y}\text{Co}_y)_2\text{As}_2$. Consequently, the value of the As-Fe-As angle ε changes less for $\text{Ba}_{1-x}\text{K}_x(\text{Fe}_{1-y}\text{Co}_y)_2\text{As}_2$ than reported for $\text{Ba}_{1-x}\text{K}_x\text{Fe}_2\text{As}_2$ and reaches only $\sim 110.5^\circ$ at $x/2 = 0.2$, where the ideal tetrahedral angle of 109.47° is found in $\text{Ba}_{1-x}\text{K}_x\text{Fe}_2\text{As}_2$. Interestingly, additional Co doping also leads to a decrease of the Fe-As distance; a reduction of $\sim 1\%$ is found for $x/2 = 0.25$ compared to only $\sim 0.3\%$ in $\text{Ba}_{1-x}\text{K}_x\text{Fe}_2\text{As}_2$.

As previously reported,²⁵ charge compensated $\text{Ba}_{0.87}\text{K}_{0.13}\text{Fe}_{1.86}\text{Co}_{0.14}\text{As}_2$ shows the tetragonal to orthorhombic phase transition, but with a reduced orthorhombic distortion compared to BaFe_2As_2 . To check how this parent like phase is influenced by increased cobalt and potassium substitution in the charge-compensated state, low temperature powder diffraction was performed. The results, depicted in Fig. 2, show that the splitting of the lattice parameters becomes weaker with increasing substitution level. The splitting is significantly reduced from $\Delta = b - a = 4\text{ pm}$ in BaFe_2As_2 to $\sim 2\text{ pm}$ for $x/2 \approx y \approx 0.07$ and 0.09 and further to $\sim 0.8\text{ pm}$ for $x/2 \approx y \approx 0.13$, where only a broadening of reflections at low temperatures is observed. Due to the diminutive size of the splitting it is difficult to determine the exact phase transition temperatures by the Rietveld method, but the general trend - a decrease of the structural phase transition temperature T_s - is clearly visible. Thus we observe a decrease of both orthorhombic distortion and phase transition temperatures with increasing substitution level $x/2 \approx y$ in charge compensated $\text{Ba}_{1-x}\text{K}_x(\text{Fe}_{1-y}\text{Co}_y)_2\text{As}_2$, which means that the structural phase transition is subsequently suppressed.

B. Magnetism

The magnetic order was microscopically studied by ^{57}Fe Mössbauer spectroscopy and muon spin relaxation on identical samples of $\text{Ba}_{1-x}\text{K}_x(\text{Fe}_{1-y}\text{Co}_y)_2\text{As}_2$.

Temperature dependent Mössbauer spectra were recorded and the temperature dependence of the iron hyperfine field $B_{\text{hf}}(T)$ was extracted. Since it is proportional to the on-site magnetic moment, it traces the magnetic order parameter for a later comparison to the structural order parameter defined by the normalized orthorhombic splitting. Representative low temperature spectra illustrating the magnetic phase transition are shown in Fig. 3. No resolved lines from magnetic nuclear Zeeman splitting can be observed even at lowest temperatures. Due to the small ordered magnetic moment and the broad field distribution resulting from the high in-plane cobalt substitution level, the onset of magnetic order is deduced directly from the line broadening seen in the raw data: Upon decreasing the temperature below the onset of the antiferromagnetic ordering, a transfer of spectral weight from the center of the paramagnetic, singlet-like resonance to its shoulders is observed. T_M^{onset} (index M for Mössbauer spectroscopy) is accordingly defined by the highest temperature below which the intensity of the central resonance starts to decrease. Below T_M^{onset} , spectra were analysed with a Gaussian distribution of effectively static iron hyperfine fields.³⁴ The error bars for the hyperfine fields given in Fig. 4 represent the widths $\sigma_{\text{hf}} = (2 \ln 2)^{-1/2} \times \text{WHM}$ of the Gaussian field distribution. Two components were used to separate magnetic (\mathcal{M}) and non-magnetic ($1-\mathcal{M}$) volume fractions: In the field distribution, the non-magnetic contribution is centered at zero with a fixed distribution width ($\langle B_{\text{hf}} \rangle = 0\text{ T}$, $\sigma_{\text{hf}} = 0.5\text{ T}$)⁸⁴ whereas the magnetic contribution displays a non-zero hyperfine field ($\langle B_{\text{hf}} \rangle \geq 0.5\text{ T}$, σ_{hf} free). The Lorentzian linewidth was fixed to its value from just above T_M^{onset} , since it is severe correlated to σ_{hf} . The magnetic volume fraction saturates at 100% for the purely magnetic samples with $x/2 \approx y = 0.07$ and 0.10 and at $\sim 45\%$ for the partially superconducting samples with $x/2 \approx y = 0.13$ and 0.16 at low temperatures. We define the antiferromagnetic transition temperature $T_N = T_M^{50\%}$ by the 50% volume fraction criterium of the low temperature saturation value. The values for $T_M^{50\%}$ are obtained from sigmoidal fits of the temperature dependence of $\mathcal{M}(T)$ and given in Tab. I. The temperature dependence of the weighted hyperfine field $B_{\text{hf}} = \langle B_{\text{hf}} \rangle \times \mathcal{M}$ is shown together with the orthorhombic splitting parameter $\delta_S = (a - b) / (a + b)$ in Fig. 4.

For all compositions, the curves of the structural and the magnetic order parameter show a remarkable proportionality. Fig. 4 shows also that the low temperature saturation value of the weighted Mössbauer hyperfine field decreases continuously with increasing Co/K-substitution: B_{hf} at $T=4.2\text{ K}$ is reduced from 5.5 T in BaFe_2As_2 ³⁵ to 3.0 T , 2.7 T , 1.4 T and 0.9 T for

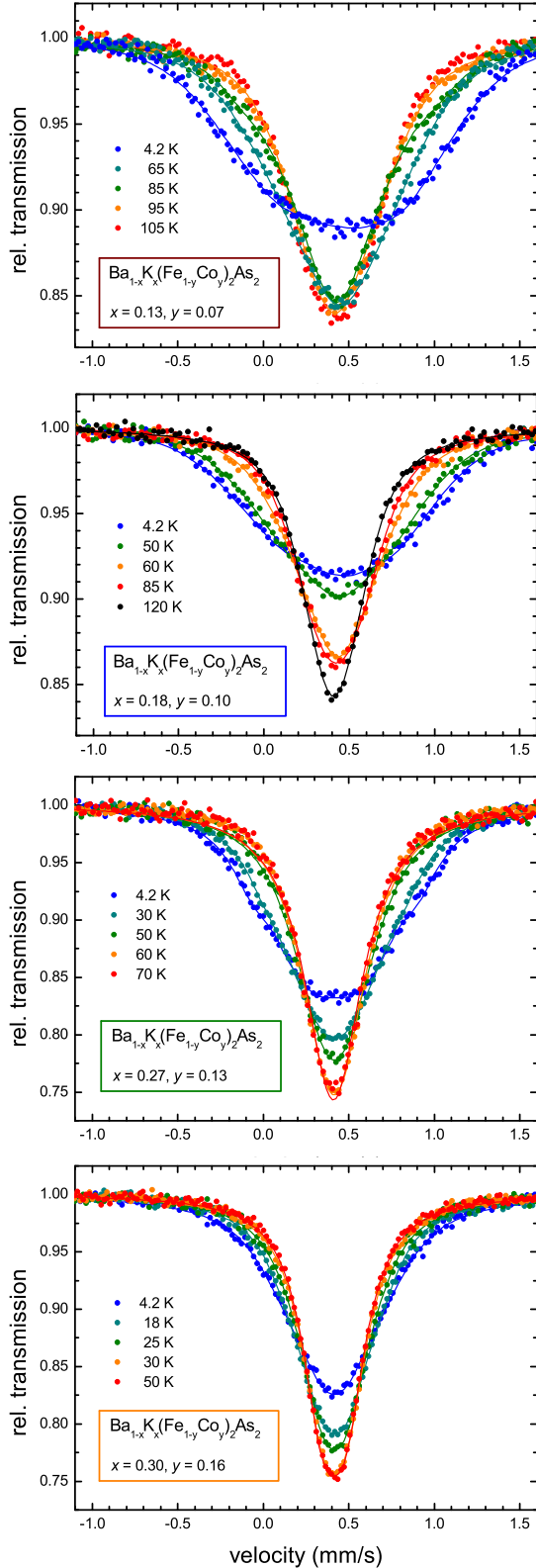


FIG. 3: Representative ^{57}Fe Mössbauer spectra of $\text{Ba}_{1-x}\text{K}_x(\text{Fe}_{1-y}\text{Co}_y)_2\text{As}_2$ for $x/2 \approx y = 0.07, 0.10, 0.13$ and 0.16 . The magnetic phase transition is evidenced by the line broadening and the concomitant transfer of spectral intensity from the central resonance to the shoulders (see text for details).

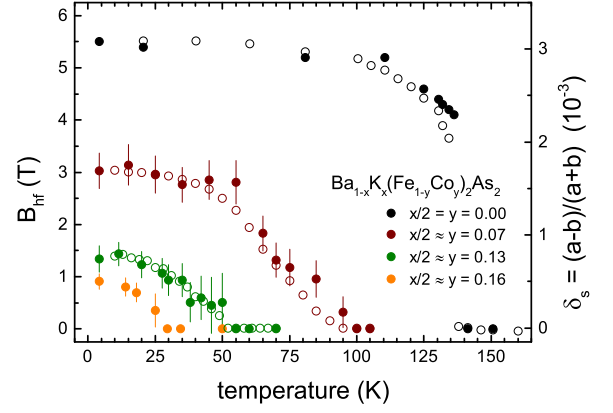


FIG. 4: Temperature dependence of the weighted hyperfine field B_{hf} (full circles, left scale) and the orthorhombic splitting parameter δ_s (open circles, right scale). Experimental data for BaFe_2As_2 ($x/2 = y = 0$) is taken from Ref.³³

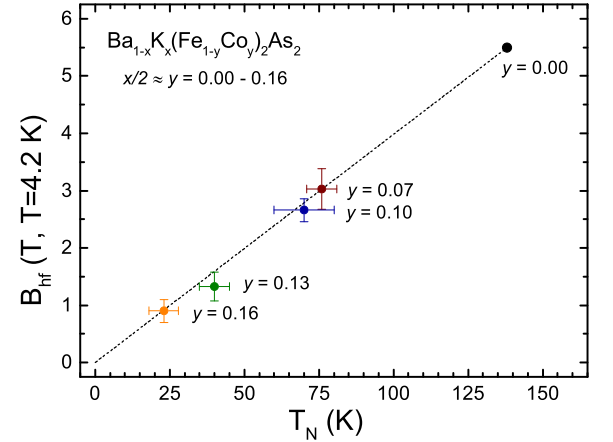


FIG. 5: The low temperature value of the weighted hyperfine field $B_{\text{hf}}(T=4.2\text{ K})$ and T_N show a linear relationship for all magnetic samples. The experimental data for BaFe_2As_2 ($y = 0$) is taken from Ref.³³

$x/2 \approx y = 0.07, 0.10, 0.13$ and 0.16 respectively. Likewise, T_N is reduced to 80 K, 70 K, 40 K and 23 K. Note that plotting $B_{\text{hf}}(4.2\text{ K})$ as a function of T_N yields a straight line that passes through the origin as shown in Fig. 5. From this we conclude, that the underlying mechanism for the magnetic ordering is identically for all compositions. Interestingly in that context is that the Mössbauer isomer shifts (IS) at 4.2 K are slightly higher in the purely magnetic samples ($\text{IS} \geq 0.52\text{ mm/s}$ for $x/2 \approx y = 0.07$ and 0.10) than in the superconducting samples ($\text{IS} \leq 0.51\text{ mm/s}$ for $x/2 \approx y = 0.13$ and 0.16), see Tab. I. This means that the local electron density at the iron site is slightly enhanced in the superconducting samples.

In order to verify our results from Mössbauer spectroscopy and the fitting model, we performed zero field (ZF) muon spin relaxation measurements (μSR) on the

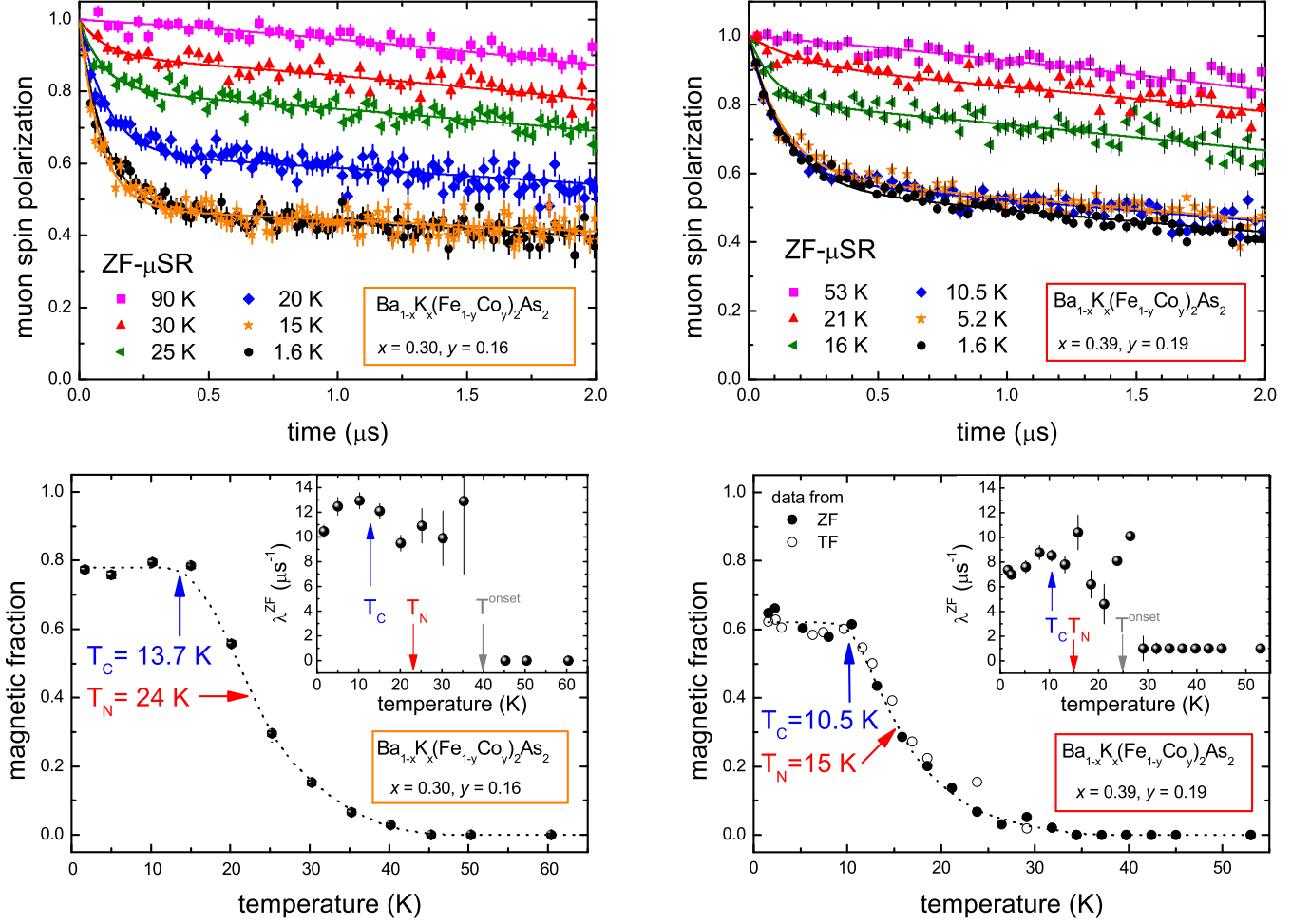


FIG. 6: Upper panels: Zero field μ SR spectra of $\text{Ba}_{1-x}\text{K}_x(\text{Fe}_{1-y}\text{Co}_y)_2\text{As}_2$ with $x/2 \approx y = 0.16$ and 0.19 . Lower panels: Extracted temperature dependencies of the corresponding magnetic volume fraction and the ZF- μ SR transverse relaxation rate λ^{ZF} (insets). Dotted lines are guides to the eyes.

sample with $x/2 \approx y = 0.16$. It has been shown, that μ SR is an excellent tool to study the volume-selective electronic properties of iron pnictides.^{15,36–39} The superconducting properties are directly accessible and μ SR is sensitive to very small ordered magnetic moments. A second sample with $x/2 \approx y = 0.19$ was also studied to confirm magnetism at higher substitution levels. In Fig. 6, zero field μ SR spectra for $x/2 \approx y = 0.16$ (upper panel left) and $x/2 \approx y = 0.19$ (upper panel right) are shown for selected temperatures. At high temperatures, both samples are characterized by a weakly damped Kubo-Toyabe depolarization ($G^{\text{LGKT}}(t, \sigma_{\text{nucl}}, \lambda_{\text{nucl}})$) which is typical for the presence of a magnetic field distribution at the muon site due to static nuclear moments only.⁴⁰ At temperatures below 40 K ($x/2 \approx y = 0.16$) or 25 K ($x/2 \approx y = 0.19$) electronic magnetism is evidenced by a strong exponential relaxation of the μ SR time spectra at early times. The absence of an oscillatory signal is associated to a broad distribution of local fields at the muon site which is typical for chemically substituted pnictides.^{37,38}

Accordingly, the time spectra were fitted (solid lines) using the function

$$P(t) = \mathcal{M} \times \{2/3 \cdot \exp(-\lambda^{\text{ZF}} \cdot t) + 1/3\} + (1 - \mathcal{M}) \times G^{\text{LGKT}}(t, \sigma_{\text{nucl}}, \lambda_{\text{nucl}}), \quad (1)$$

where \mathcal{M} is the magnetic volume fraction and λ^{ZF} the magnetic ZF- μ SR relaxation rate. The nuclear depolarization rates indexed by 'nucl' were fitted for all temperatures simultaneously to avoid a parameter correlation with the magnetic ZF- μ SR relaxation rate. It is important to note that using ZF- μ SR, the magnetic volume fraction \mathcal{M} can be determined with high accuracy, *viz.* within an error range of a few percent.

The magnetic transition is gradual in temperature as seen by the increase of the magnetic volume fraction in Fig.6 (bottom). As an estimate for the Néel temperature we define –analogue to Mössbauer spectroscopy– T_N as the temperature at which 50% of the sample is magnetically ordered with respect to the low tempera-

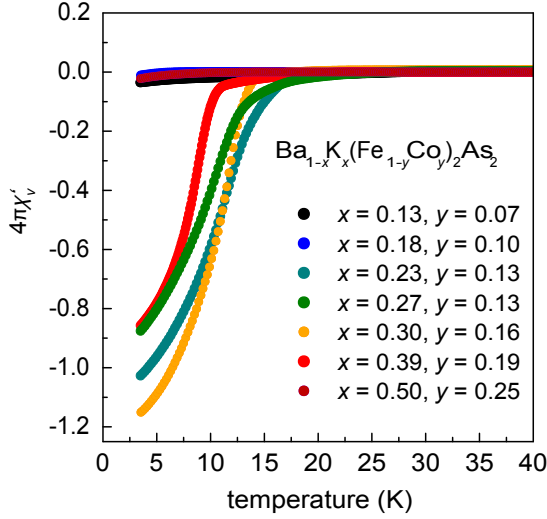


FIG. 7: Real part of the ac susceptibility signal for charge compensated $\text{Ba}_{1-x}\text{K}_x(\text{Fe}_{1-y}\text{Co}_y)_2\text{As}_2$. For substitution levels $x/2 \approx y$ between 0.13 and 0.19, bulk superconductivity is found.

ture saturation value. We obtain $T_\mu^{50\%} = 24$ K for $x/2 \approx y = 0.16$ in agreement with Mössbauer spectroscopy and $T_\mu^{50\%} = 15$ K for $x/2 \approx y = 0.19$.

For both samples, the ZF- μ SR transverse relaxation rate λ^{ZF} shows a maximum at T_c obtained from ac-susceptibility with a following decrease towards low temperatures. Also at T_c , the magnetic volume fraction ceases to increase and remains constant towards lower temperatures. The combination of these two anomalies is reminiscent of the decrease of the magnetic order parameter seen in $\text{Ba}_{1-x}\text{K}_x\text{Fe}_2\text{As}_2$ ¹⁵ and $\text{Ba}(\text{Fe}_{1-x}\text{Co}_x)_2\text{As}_2$ ^{37,38} at the onset of superconductivity and indicates that magnetism and superconductivity compete for the same electrons.

C. Superconductivity

Measurements of the ac susceptibility (see Fig. 7) confirm *bulk* superconductivity for charge compensated $\text{Ba}_{1-x}\text{K}_x(\text{Fe}_{1-y}\text{Co}_y)_2\text{As}_2$ with a substitution level ranging from $x/2 \approx y = 0.13$ to 0.19. Finally at $x/2 \approx y = 0.25$, we observe no more diamagnetic response signal, which shows that the superconducting dome spans about 10% in the cobalt content.

From the low temperature value of χ' , we estimate the superconducting volume fraction \mathcal{S} for a quantitative comparison to the magnetic volume fraction \mathcal{M} extracted from ZF- μ SR: Even if we assume that due to demagnetization corrections \mathcal{S} only becomes 100% for $4\pi\chi'_v = -1.5$, we find a lower boundary for the superconducting volume fraction of $\mathcal{S} = 0.9$ for the sample with $x/2 \approx y = 0.16$ (Fig. 7, yellow curve) and $\mathcal{S} = 0.7$ for the sample with $x/2 \approx y = 0.19$ (Fig. 7, red curve). A comparison with the magnetic volume fractions \mathcal{M} of the identical sam-

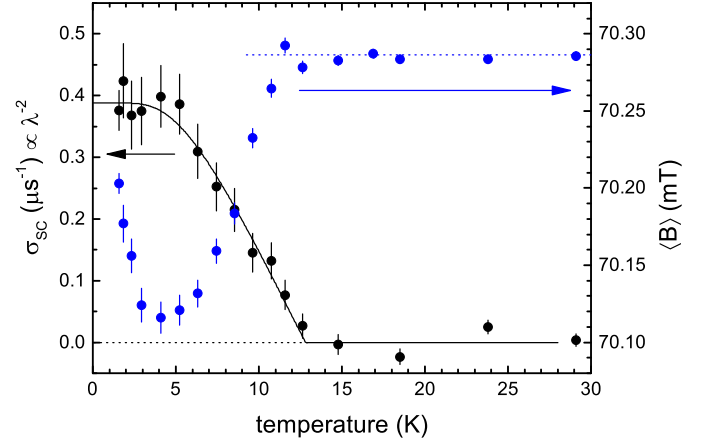


FIG. 8: Temperature dependence of the local field $\langle B \rangle$ (blue dots) and the vortex lattice relaxation rate σ_{SC} (black dots) within the non-magnetic volume fraction of $\text{Ba}_{0.62}\text{K}_{0.38}\text{Fe}_{1.62}\text{Co}_{0.38}\text{As}_2$ ($x/2 \approx y = 0.19$) as determined by a transverse field experiment. The solid black line is a fit within a single s-wave gap scenario (see text for details).

ples which we precisely determined using ZF- μ SR (see Fig. 6) yields $\mathcal{M} = 0.8$, $\mathcal{S} = 0.9$ for $x/2 \approx y = 0.16$ and $\mathcal{M} = 0.6$, $\mathcal{S} = 0.7$ for $x/2 \approx y = 0.19$. Thus, the overlap of the superconducting and magnetic volume is at least 70% for a substitution level of $x/2 \approx y = 0.16$ and 30% for a substitution level of $x/2 \approx y = 0.19$. Together with the maximum of the ZF- μ SR transverse relaxation rate λ^{ZF} which we observe at T_c in both samples, we conclude from these values that in charge compensated $\text{Ba}_{1-x}\text{K}_x(\text{Fe}_{1-y}\text{Co}_y)_2\text{As}_2$, superconductivity and magnetism coexist *microscopically* at least in a partial volume fraction.

For $x/2 \approx y = 0.19$ we performed transverse field (TF) μ SR experiments to study the superconducting properties of the non-magnetic volume fraction ($1-\mathcal{M}$) in detail. In a type-II superconductor, one measures the probability distribution $n(B)$ in the vortex state.^{41–43} Its first moment, the measured averaged magnetic field $\langle B \rangle$ at the muon site is given by the oscillating frequency in the μ SR time spectrum. Electronic and nuclear dipolar fields as well as the spin polarization of the conduction electrons at the muon site result in a shift of $\langle B \rangle$ with respect to the applied external field, known as (muon) Knight shift. For polycrystalline samples, the field distribution from the vortex lattice (VL) can be approximated using a Gaussian function. Therefore, VL formation causes an additional gaussian relaxation rate σ_{SC} in the time domain. From its temperature dependence⁸⁵ one can estimate the London penetration depth λ for $T \rightarrow 0$ via the Brandt formula $\sigma_{\text{SC}}^2 = 0.00371 \Phi_0^2 / \lambda^4$.⁴¹

Both measured quantities $\langle B \rangle$ and σ_{SC} are shown together in Fig. 8. In the non-superconducting (normal) state above ~ 12 K, $\langle B \rangle$ remains constant. For polycrystalline iron-pnictides, this value is typically slightly smaller than the applied external field yielding a nega-

tive normal-state Knight shift.⁴⁴ The downturn of $\langle B \rangle$ below ~ 12 K (Meissner effect) is accompanied by the appearance of increasing σ_{SC} in the μ SR time spectra and confirm microscopically the superconducting phase transition determined by ac susceptibility measurements ($T_{C,acs} = 10.5$ K, see Fig. 7). The origin of the upturn of $\langle B \rangle$ below ~ 4 K cannot be conclusively explained. Most likely, it may be associated to a Yosida-like⁴⁵ decrease of the spin-susceptibility which is concealed by the diamagnetic shielding at temperatures between 4 and 12 K. Also field induced magnetism,^{46,47} vortex disorder⁴³ or other effects might cause this anomaly. This topic is worth to study separately in detail if big enough single crystals of $Ba_{1-x}K_x(Fe_{1-y}Co_y)_2As_2$ become available. The temperature dependence of σ_{SC} shown in Fig. 8 suggests a nodeless symmetry for the superconducting order parameter. Our data is compatible with a BCS-like single s-wave gap scenario and a corresponding fit^{48,49} (solid black line) yields $\lambda(0) = 280$ nm and a gap value of $\Delta = 1$ meV for $T_c = 13$ K. From these values, we calculate the BCS coupling ratio $2\Delta/k_B T_c = 1.9$ which agrees well to literature data for values of the so-called "smaller gap" observed in various iron pnictide systems.^{46,49}

D. Band Structure Calculations

To study the development of the electronic and magnetic properties of the $Ba_{1-x}K_x(Fe_{1-y}Co_y)_2As_2$ compounds, we performed a series of density functional calculations in different approximations. In a simple rigid band picture, a charge compensated substitution ($x/2 = y$) would not yield any changes of the related electronic structure, apart from changes caused by the slight modifications of the crystal structure (see Fig. 1). Therefore, we applied a virtual crystal approximation (VCA) for both the Ba- and the Fe-sites. Since Ba and K act essentially as a charge donor on the A-site in the AFe_2As_2 compounds, and Fe and Co behave rather similar with respect to their bonding behavior, a VCA approach should describe the change of the averaged crystal potential in good approximation. (To simulate the changed electron count due to the Ba-K substitution, only the number of Ba valence electrons was reduced according to the K content, disregarding the different core electrons of both elements.) Since the translation symmetry of the unit cell is preserved, the direct influence of the substitution related scattering on the electronic structure is neglected. This will be part of a future study.

The charge compensated Fe-Co/Ba-K substitution in $Ba_{1-x}K_x(Fe_{1-y}Co_y)_2As_2$ leads to a fast suppression of the ordered magnetic moment in the stripe antiferromagnetic state with increasing $x/2 = y$ (see upper panel of Fig. 10, open squares). Our calculations yield a fast, essentially linear decrease of the Fe magnetic moment with increasing Co/K substitution, followed by a sudden drop and the complete breakdown of the stripe AFM order at about $x/2 = y \approx 0.15$. This result agrees well with the

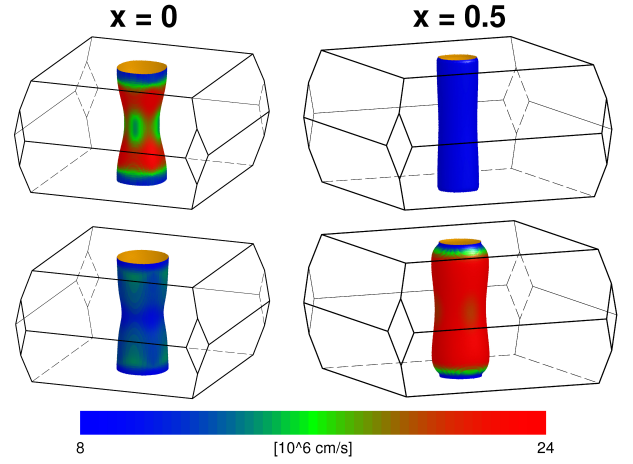


FIG. 9: The calculated hole-related Fermi surface sheets of $Ba_{1-x}K_x(Fe_{1-y}Co_y)_2As_2$ for $x = y = 0$ (left panel) and $x/2 = y = 0.25$ (right panel). The respective Fermi velocities are indicated by the color-mapping. The shape of the electron surfaces is essentially unchanged in both compounds.

suppression of the measured low temperature saturation value for the weighted Mössbauer hyperfine field B_{hf} (see Fig. 10, filled circles). To compare the calculated and experimental Fe moment, B_{hf} is scaled by a constant factor so that both values match the one of the unsubstituted $BaFe_2As_2$ compound.

A closer look onto the related changes of the calculated electronic structure reveals sizable differences in the shape of the Fermi surfaces (see Fig. 9, non-magnetic calculations of the simple tetragonal cell for $x/2 = y = 0$ and $x/2 = y = 0.25$), in particular the hole-related sheets. The suppression of the AFM stripe order for $y \geq 0.15$ is likely, at least in part, caused by the reduced nesting of the Fermi surfaces. Another manifestation of the changes in the band structure is shown by the electronic density of states (DOS) N at the Fermi level ε_F : Increasing substitution y results in a sizable reduction of $N(\varepsilon_F)$ which can be assigned predominantly to the Fe $3d$ states (see Fig. 10, lower panel). Interestingly, the suppression of the magnetic moment is well compatible with a naive Stoner-like picture. According to the Stoner criterion, which yields a magnetic instability by a divergency of $\chi = \chi_0/(1 - IN(\varepsilon_F))$ if $IN(\varepsilon_F) \leq 1$, a magnetic ground state would be expected for small y : For Fe- $3d$ states with $I \sim 1 \pm 0.1$, the Stoner criterion is only fulfilled for $N(\varepsilon_F) \geq 1/I$ which is marked by the dashed lines in Fig. 10. Even if the Stoner criterion is not directly applicable for the formation of the AFM stripe order that involves Fermi surface nesting, it provides at least a qualitative picture for the development of a magnetic instability with respect to Fe-Co/Ba-K substitution and suggests, why the AFM stripe order is not replaced by a simple FM order when this substitution suppresses the nesting.

In addition to the study of the Fermi surfaces and suppression of the stripe-order magnetism, we tried to

Sample No.		N27	N43	N47	N45	N46
Low temperature state	afm	afm	afm	afm+sc	afm+sc	afm+sc
K-substitution	$x = 0.00$	$x = 0.13$	$x = 0.18$	$x = 0.27$	$x = 0.30$	$x = 0.39$
Co-substitution	$y = 0.00$	$y = 0.07$	$y = 0.10$	$y = 0.13$	$y = 0.16$	$y = 0.19$
$T_{c,acs}$ [K]	0	0	0	14	13.7	10.5
$T_{S,x-ray}$ [K]	140	90	105	50	0	0
$T_M^{onset} \mid T_\mu^{onset}$ [K]	155	95(5)	100(10)	50(5) -	29(5) 40	- 25
$T_N = T_M^{50\%} \mid T_\mu^{50\%}$ [K]	138	76(5)	70(10)	40(5) -	23(5) 24	- 15
$B_{hf}(4.2\text{ K})$ [T]	5.5	3.0(1)	2.7(1)	1.4(1)	0.9(1)	-
$B_{hf}(4.2\text{ K})/T_M^{50\%}$ [T/K]	0.04	0.039(4)	0.039(7)	0.035(6)	0.038(8)	-
IS(4.2 K) [mm/s]	0.53(1)	0.531(5)	0.526(5)	0.509(5)	0.504(5)	-
$\epsilon(4.2\text{ K})$ [mm/s]	-0.04(1)	-0.030(10)	-0.030(12)	-0.034(15)	-0.030(15)	-
$\Gamma/2(293\text{ K})$ [mm/s]	0.155	0.18(1)	0.15(1)	0.15(1)	0.14(1)	-

TABLE I: Transition temperatures from x-ray diffraction, ac-susceptibility and muon spin relaxation along with selective hyperfine parameters for $\text{Ba}_{1-x}\text{K}_x(\text{Fe}_{1-y}\text{Co}_y)_2\text{As}_2$ derived from Mössbauer spectroscopy measurements. The isomer shift IS is given relative to metallic iron; $\epsilon = (e^2qQ/2)$ is the effective quadrupole shift. Data for BaFe_2As_2 are taken from Refs.^{33,35}

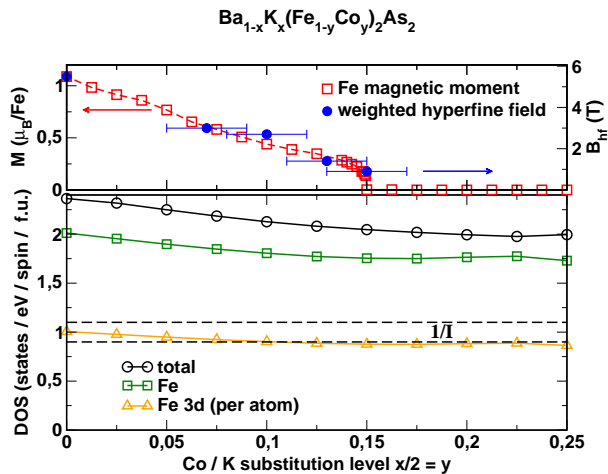


FIG. 10: Upper panel: Calculated magnetic moment (per Fe) in the antiferromagnetic "stripe" phase as a function of the Co / K substitution level $x/2 = y$ in $\text{Ba}_{1-x}\text{K}_x(\text{Fe}_{1-y}\text{Co}_y)_2\text{As}_2$ together with the weighted hyperfine field B_{hf} ($T=4.2\text{ K}$). The measured hyperfine fields are scaled by a constant factor to match the calculated Fe-moment for the undoped parent compound BaFe_2As_2 . Lower panel: Total and partial electronic density of states (DOS) at the Fermi level for $\text{Ba}_{1-x}\text{K}_x(\text{Fe}_{1-y}\text{Co}_y)_2\text{As}_2$ for non-magnetic calculations. With increasing substitution level the DOS decreases, and for $y \geq 0.11$ the Fe-3d contribution (per Fe atom and spin) drops below the Stoner criterion for a magnetic instability (marked by the dashed lines for $I(\text{Fe-3d}) = 1 \pm 0.1$, see text).

separate the influence of the substitution related structural changes (see Fig. 1) on the electronic structure and the influence of the change of the averaged crystal potential, which was discussed in previous studies.²⁴ This change originates from the different charge distribution within and between the Fe-As layers caused by the varying (charge compensated) Fe-Co/Ba-K substitution. To this aim, we carried out calculations where (i) only the structure of the parent compound BaFe_2As_2 was changed simulating the experimentally observed crystal structure (see Fig. 1), (ii) substitution only was simulated by the VCA approach keeping the structure of the unsubstituted BaFe_2As_2 , and (iii) calculations for the "real" compounds combining (i) and (ii). Our calculations indicate that the dominant contribution to the changes of the electronic properties is due to substitution (ii); the structural changes, in particular the elongation of the c axis, play a minor role. Interestingly, the total changes of the DOS $N(\varepsilon_F)$ in the full calculation (iii) can be represented as the sum of the changes from (i) and (ii) with high accuracy. This supports the idea that both effects are rather independent and offers the opportunity to fine-tune this type of compound, for instance by applying uniaxial or hydrostatic pressure.

IV. DISCUSSION

As we have shown in the previous section, charge compensated $\text{Ba}_{1-x}\text{K}_x(\text{Fe}_{1-y}\text{Co}_y)_2\text{As}_2$ with a low substitution level ($x/2 \approx y \leq 0.10$) displays a parent-like antiferromagnetic and orthorhombic state at low temperatures within the whole sample volume. The magnitude of the ordered, magnetic moment and likewise the orthorhombic distortion is subsequently suppressed upon increasing the Co/K substitution level $x/2 \approx y$ (denoted as y in the following). Using microscopic techniques, we show that magnetism persists up to $y = 0.19$ whereas the orthorhombic distortion is only detected up to $y = 0.13$. The onset of magnetic order and structural distortion occur at the same temperature and our data prove a temperature independent, linear relationship between the normalized orthorhombic splitting δ_s and the weighted hyperfine field B_{hf} , *i.e.* between the magnetic and structural order parameter. The suppression of the ordered moment is well reproduced by our DFT calculations. Furthermore, we find bulk superconductivity for $0.13 \leq y \leq 0.19$. For the samples with $y = 0.16$ and 0.19 , we conclude from ZF- μSR and ac susceptibility data, that magnetism and superconductivity coexist microscopically in a large fraction of the sample volume.

A. Magnetism

For charge compensated $\text{Ba}_{1-x}\text{K}_x(\text{Fe}_{1-y}\text{Co}_y)_2\text{As}_2$, we discuss the suppression of magnetism upon increasing the Co/K substitution level by a comparison to the well-studied, nominally isovalent $\text{Ba}(\text{Fe}_{1-x}\text{Ru}_x)_2\text{As}_2$ system^{50–54} because both systems show significant common properties:

The concomitant onset of magnetic order at the structural transition temperature in $\text{Ba}_{1-x}\text{K}_x(\text{Fe}_{1-y}\text{Co}_y)_2\text{As}_2$ is reminiscent of the common temperatures for the magnetic and structural phase transition in $\text{Ba}(\text{Fe}_{1-x}\text{Ru}_x)_2\text{As}_2$,⁵² and will be discussed separately in section IV C. The suppression of the ordered magnetic moment as a function of chemical substitution in both systems displays a linear behaviour shown in Fig. 11. Both observables for the magnetic order parameter (B_{hf} for $T=4.2\text{ K}$ from this work and M for $T \rightarrow 0$ from Ref.⁵¹) are normalized to their values in the common pristine system BaFe_2As_2 and the chemical substitution axes were scaled by a factor of ~ 1.5 in order to get a maximum correspondence. We attribute the fact that less Co/K than Ru substitution is necessary to suppress the magnetic moment in the same way to the different sizes of the Ru 4d and the Fe/Co 3d orbitals. Since the Ru 4d orbitals are spatially more extended, the itinerant magnetism is more stable against partial substitution. Note, that a recent XRD study reports that Ru is spin-polarized with a Ru L_2 edge signal that follows the magnetic ordering of Fe with an in-plane correlation length corresponding to more than 700 unit cells.⁵⁴ This may

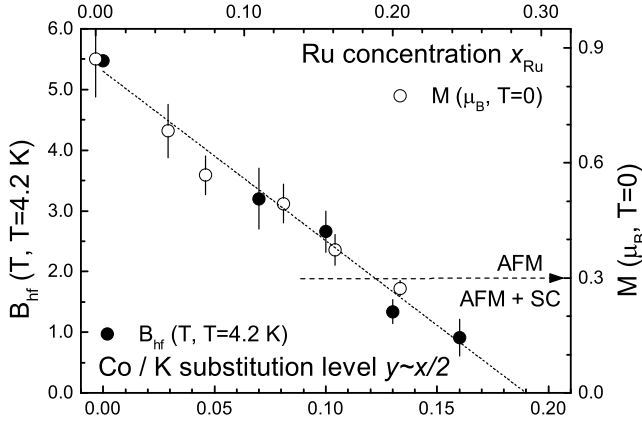


FIG. 11: Ordered magnetic moment at low temperatures in $\text{Ba}_{1-x}\text{K}_x(\text{Fe}_{1-y}\text{Co}_y)_2\text{As}_2$ (B_{hf} for $T=4.2$ K from this work, bottom/left axes) and $\text{Ba}(\text{Fe}_{1-x}\text{Ru}_x)_2\text{As}_2$ (M for $T \rightarrow 0$ from Ref.⁵¹, top/right axes). Both systems show a linear dependence upon chemical substitution.

also stabilize the AFM order. In contrast to Ru substitution, Co shows no signatures of spontaneous or induced spin polarization as probed by a combined ^{59}Co and ^{75}As NMR study of $\text{Ba}(\text{Fe}_{1.8}\text{Co}_{0.2})_2\text{As}_2$.⁵⁵

Fig. 11 reveals two further similarities between both systems: Firstly, superconductivity emerges at a substitution level of $\tilde{y} \sim 0.12$ for $\text{Ba}_{1-x}\text{K}_x(\text{Fe}_{1-y}\text{Co}_y)_2\text{As}_2$ and $\tilde{x}_{\text{Ru}} \sim 0.18$ for $\text{Ba}(\text{Fe}_{1-x}\text{Ru}_x)_2\text{As}_2$, respectively, for which the ordered magnetic moment μ has fallen below a 'critical' value of $\tilde{\mu} = 0.3 \mu_B$ (dashed arrow). This will be discussed in section IV B below. Secondly, a linear extrapolation of the ordered macroscopic averaged magnetic moments (dotted lines) yields values for the corresponding substitution levels close to $x_{\text{Ru}} \sim 0.3$ and $y \sim 0.2$ above which the magnetism is suppressed in both systems. In the $\text{Ba}(\text{Fe}_{1-x}\text{Ru}_x)_2\text{As}_2$ system, Laplace et al. consider this substitution level (25% – 35%) to be the percolation threshold for magnetic ordering.⁵⁰ They also point out, that it is of importance to differentiate between the nominal (macroscopic average) and local (microscopic average) substitution levels x_{nom} and x_{loc} depending on how the electronic properties are determined. The Fe layer properties are assumed to be governed by x_{loc} which may differ from x_{nom} . For $\text{Ba}(\text{Fe}_{1-x}\text{Ru}_x)_2\text{As}_2$, they conclude an intrinsically *inhomogeneous* electronic state on a local scale which accounts for the coexistence of superconductivity and magnetism. This is in contrast to $\text{Ba}(\text{Fe}_{1-x}\text{Co}_x)_2\text{As}_2$, where *homogeneous* coexistence between superconductivity and magnetism was deduced from the interplay of the superconducting and magnetic order parameter.¹⁴ For charge compensated $\text{Ba}_{1-x}\text{K}_x(\text{Fe}_{1-y}\text{Co}_y)_2\text{As}_2$ with a substitution level of $y = 0.16$ and 0.19 , our data shows microscopic coexistence of magnetic and superconducting based on the overlap of the magnetic and superconducting volume fractions at low temperatures. However, the

experimental evidence for the interplay of both order parameters *cf.* the reduction of the magnetic ZF- μSR transverse relaxation rate λ^{ZF} below T_c is weak (see inset of Fig. 6) and has to be studied in more detail. Nevertheless, our results support an homogeneous scenario.

The results of our DFT calculations on $\text{Ba}_{1-x}\text{K}_x(\text{Fe}_{1-y}\text{Co}_y)_2\text{As}_2$ quantitatively reproduce the experimentally observed suppression of the ordered magnetic moment upon decreasing y (see Fig. 10). They also show, that the weakening of magnetism can be directly related to a reduced density of states at the Fermi level consistent to earlier calculations on the endpoint of the $x/2 = y$ series (KFeCoAs_2 , $y = 0.5$).⁵⁶ There, the weakening of magnetism was also found as a result of the reduction in the density of states at the Fermi energy $N(\varepsilon_F)$ and this change has been attributed to a shrinking of the in-plane lattice parameter a . However, our three-fold DFT study clearly shows, that structural changes are less important for the reduction of $N(\varepsilon_F)$ compared to the effects of chemical (double-)substitution. Furthermore, our results point to a Stoner-like development of the magnetic instability. One may understand this in the context of recent results from a valence band photoemission and Auger Electron Spectroscopy study,²¹ showing that Co states have significant Fe 3d character with an almost negligible increased effective onsite Coulomb interaction U_{eff} . In that work, Kraus et. al. showed also that transition metal states move to higher binding energies with increasing atomic number, contributing less and less to the states close to the Fermi level. From this findings, we deduce that for an in-plane substitution with Co, the density of states $N(\varepsilon_F)$ is a good quantity for determining the strength of magnetism in charge compensated $\text{Ba}_{1-x}\text{K}_x(\text{Fe}_{1-y}\text{Co}_y)_2\text{As}_2$. An effective itinerant scenario for the description of the magnetic instability was also proposed for $\text{Ba}(\text{Fe}_{1-x}\text{Ru}_x)_2\text{As}_2$.⁵³ In that work, Dhaka et al. suggested, that either magnetic dilution and the associated reduction of an effective Stoner enhancement or the enhancement of impurity scattering leads to the suppression of the magnetic order. We want to emphasize, that the seemingly contradiction of a random *local* defect being responsible for a change in the quantities of an *itinerant* model was reconciled by Berlijn et al.¹⁹

B. Superconductivity

Our results for the shape and the position of the superconducting dome in charge compensated $\text{Ba}_{1-x}\text{K}_x(\text{Fe}_{1-y}\text{Co}_y)_2\text{As}_2$ agree with the results by Suzuki et al.²⁴ based on resistivity measurements. However, they report a *non-magnetic* superconducting phase for $0.1 \leq y \leq 0.2$ which contradicts our observation of a finite Mössbauer hyperfine field B_{hf} measured on samples with $y = 0.13$ and 0.16 and the magnetic relaxation in the ZF- μSR time spectra for $y = 0.16$ and 0.19 . Never-

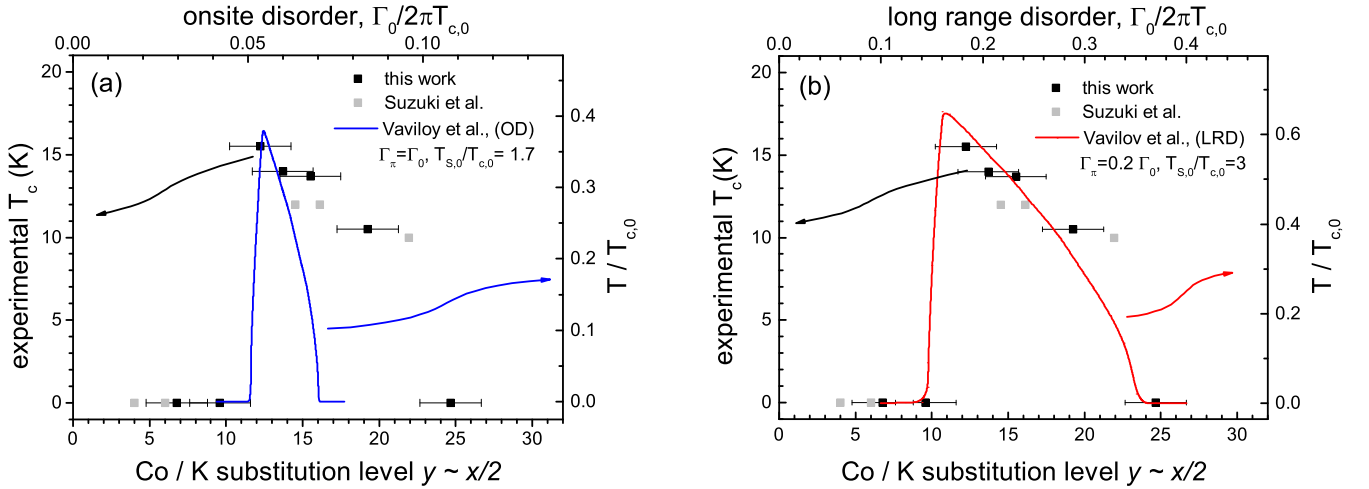


FIG. 12: Comparison of experimental (T_c from this work in black and Ref.²⁴ in gray) and calculated ($T/T_{c,0}$ from Ref.⁵⁷) transition temperatures under the assumption that $\Gamma_0/2\pi T_{c,0} \propto n_{\text{imp}} \propto y$. (a) Best possible scaling to a pure *interband* scattering scenario (OD, blue line). (b) Best possible scaling to a dominantly *intra*band scattering scenario (LRD, red line).

theless, resistivity measurements may not be sensitive to weak magnetic order and therefore, it is possible that superconductivity and magnetism coexist on a microscopic length scale.

The onset of superconductivity in charge compensated $\text{Ba}_{1-x}\text{K}_x(\text{Fe}_{1-y}\text{Co}_y)_2\text{As}_2$ occurs at a substitution level y between 0.10 and 0.13. As we show in Fig. 11, the comparison of the ordered magnetic moment to the $\text{Ba}(\text{Fe}_{1-x}\text{Ru}_x)_2\text{As}_2$ system yields a substitution level of $\tilde{y} \sim 0.12$ above which the ordered magnetic moment has fallen below a 'critical' value of $\tilde{\mu} = 0.3 \mu_B$ ⁵⁰ giving rise to superconductivity. The value of $\tilde{\mu} = 0.3 \mu_B$ is also found in electron-doped $\text{Ba}(\text{Fe}_{1-x}\text{Co}_x)_2\text{As}_2$ for a substitution level of $\tilde{x}_{\text{Co}} \sim 0.05$, above which coexistence and competition between superconductivity and magnetism is reported.⁵⁸ This is inline with the overall evidence, that for electron doped transition metal-substituted Fe-based 122 superconductors, the substitution level is the salient parameter for the suppression of the magnetic and structural transition to a low-enough temperature, which is a necessary condition for the appearance of superconductivity. However, the span of the superconducting dome is appropriately described using the nominal electron count e ,^{10,59} but only as long as a rigid band picture holds and as long as the transition-metal impurity potential shift is small, *viz.* only for cobalt substitution.²⁰ For systems with effectively isovalent substitution, e has no physical meaning and thus the changes of the electronic properties must be effectively related to the substitution level. We thus conclude, that for charge compensated $\text{Ba}_{1-x}\text{K}_x(\text{Fe}_{1-y}\text{Co}_y)_2\text{As}_2$, the superconducting transition temperature T_c is essentially depending on the substitution level y or in other words, by the density of in-plane impurities.

Vavilov and Chubukov consider the effect of non-magnetic impurities without a change of the density of

carriers for iron-pnictides.⁵⁷ They conclude that the spin density wave (SDW) order is suppressed stronger than s^\pm -superconductivity, because intra- and interband scattering is destructive for SDW, but only interband scattering is pair-breaking for an s^\pm -superconductor. Since the disorder parameter $\Gamma_0/2\pi T_{c,0}$ introduced by Vavilov and Chubukov in their work is proportional to the impurity density n_{imp} , we assume that (i) qualitatively, $\text{Ba}_{1-x}\text{K}_x(\text{Fe}_{1-y}\text{Co}_y)_2\text{As}_2$ with $x/2 = y$ is an experimentally accessible system for this theory and (ii) that quantitatively, $\Gamma_0/2\pi T_{c,0}$ is proportional to the Co/K substitution level y . In Fig. 12, we compare experimental (T_c) and calculated ($T/T_{c,0}$) transition temperatures for a pure interband scattering (onsite disorder (OD), $\Gamma_0 = \Gamma_\pi$) and a dominantly interband scattering (long range disorder (LRD), $\Gamma_0 = 5 \Gamma_\pi$) scenario discussed in Ref.⁵⁷. We find good agreement for the shape of the superconducting dome within the LRD scenario whereas no suitable scaling could be achieved for OD. The value for $T_{S,0}/T_{c,0} = 3$ used in the LRD is reasonable for $\text{Ba}_{1-x}\text{K}_x(\text{Fe}_{1-y}\text{Co}_y)_2\text{As}_2$ since $T_{S,0} \sim 140$ K in BaFe_2As_2 and $T_{S,0} \sim 40$ K in $\text{Ba}_{1-x}\text{K}_x\text{Fe}_2\text{As}_2$.

Clearly, a picture in which the quasi-particle scattering is due to dominantly *intra*band processes describes our data for charge compensated $\text{Ba}_{1-x}\text{K}_x(\text{Fe}_{1-y}\text{Co}_y)_2\text{As}_2$ better. However, both theoretical scenarios predict only a very narrow range Δy for a mixed SC and SDW phase (corresponding to $\Delta y < 0.02$) while our experimental findings show coexistence for a quite broad range ($\Delta y \approx 0.10$).

C. Interplay between Magnetism and Structural Distortion

We now discuss the interplay between magnetism and the orthorhombic distortion in charge compensated $\text{Ba}_{1-x}\text{K}_x(\text{Fe}_{1-y}\text{Co}_y)_2\text{As}_2$. As shown in Fig. 4, we observe no difference between the structural transition and the onset of magnetic order within experimental resolution. Although the 50% criterion in our definition of T_N leads to a separation of the magnetic and structural phase transition temperatures, our x-ray and Mössbauer data clearly show emerging magnetism directly below the structural phase transition, similar to the pristine system BaFe_2As_2 .^{35,60} In contrast, Suzuki et. al. reported a separation of both transitions based on macroscopic resistivity measurements.²⁴ The closeness of the structural and the magnetic transition in our samples is better seen if one plots the weighted Mössbauer hyperfine field B_{hf} as a function of the orthorhombic splitting δ_S , as shown in Fig. 13.

A linear relationship which extrapolates to zero between both quantities becomes evident for charge compensated $\text{Ba}_{1-x}\text{K}_x(\text{Fe}_{1-y}\text{Co}_y)_2\text{As}_2$. A corresponding fit yields 1.5 T per 10^{-3} for the slope and a negligible value ($< 10^{-4}$) for the intercept. This implies that $T_N \approx T_S$ which is a common property of the 122 parent systems BaFe_2As_2 , SrFe_2As_2 , EuFe_2As_2 , CaFe_2As_2 and also nominally charge isovalent $\text{Ba}(\text{Fe}_{1-x}\text{Ru}_x)_2\text{As}_2$. Furthermore, Fig. 13 shows that the low temperature values for the orthorhombic splitting and the ordered magnetic moment of all these systems lie on the same line. In case of magnetic rare earths, values above the rare earth ordering temperature were taken to avoid effects caused by the interplay of rare earth and iron magnetism.⁶¹ Note that for the 1111 systems where $T_S > T_N$, all mentioned compounds have comparable low temperature values for the structural distortion and ordered iron moment, in stark contrast to the 122 systems where $T_S \approx T_N$. References for the literature data used in Fig. 13 is given in Tab. II. We also added temperature dependent data for BaFe_2As_2 and SrFe_2As_2 to emphasize the linear relationship between the magnetic and structural order parameter we find in $\text{Ba}_{1-x}\text{K}_x(\text{Fe}_{1-y}\text{Co}_y)_2\text{As}_2$.

The implications of the proportionality of the structural and magnetic order parameter in the iron pnictides were firstly addressed by Wilson et al.⁶² Their analysis of the critical behaviour shows 2D Ising magnetism in $T_N = T_S$ -materials which transition to a 3D Ising-like character once the structural and magnetic transition are decoupled from each other. Cano et al.⁶³ included harmonic magneto-elastic coupling in the free energy of a Ginzburg-Landau approach and concluded that the difference between the structural and the magnetic transition temperature is crucial for the character of the corresponding phase transition. If T_S is much larger than T_N , as it is the case in undoped 1111 systems (illustrated by the finite intercept for LaOFeAs in Fig. 13), both transitions are of second order. If both transition temperatures

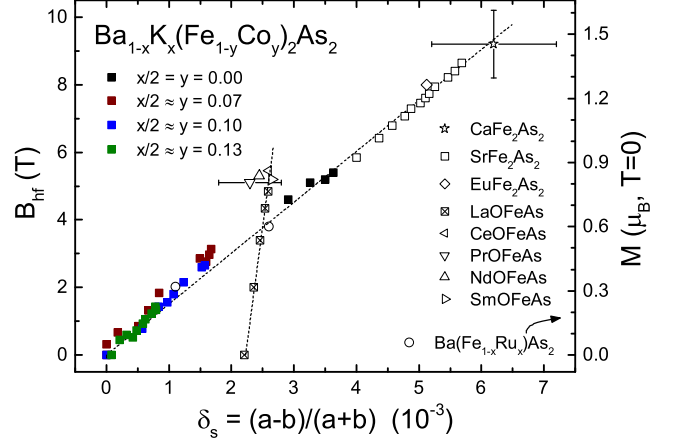


FIG. 13: Ordered Fe magnetic moment measured by B_{hf} as function of the orthorhombic splitting parameter δ_s for $\text{Ba}_{1-x}\text{K}_x(\text{Fe}_{1-y}\text{Co}_y)_2\text{As}_2$ with $x/2 \approx y$ (same data and colors as in Fig. 4) together with literature data for various nominal charge equivalent 122 and 1111 systems. References are given in Tab. II. In the case of $\text{Ba}(\text{Fe}_{1-x}\text{Ru}_x)_2\text{As}_2$, the magnetic moment was taken from neutron diffraction data and scaled identically to Fig. 11. Experimental error bars of our data have been omitted for clarity; error bars are only given for CaFe_2As_2 and PrOFeAs , where available data differ by more than 10%. Dotted lines are guides to the eyes.

become closer to each other, the magnetic part of the split transition eventually becomes first-order.

In charge compensated $\text{Ba}_{1-x}\text{K}_x(\text{Fe}_{1-y}\text{Co}_y)_2\text{As}_2$ (see Fig. 4) as well as in $\text{Ba}(\text{Fe}_{1-x}\text{Ru}_x)_2\text{As}_2$ (Fig. 3 and 4 in Ref.⁵²) at an intermediate K/Co substitution level or Ru concentration respectively, both transitions are more gradual compared to the step-like transition in the common parent compound BaFe_2As_2 in which a second-order structural transition is followed by a first-order magnetic transition with $T_S > T_N$.⁶⁰ For the case of Ru substitution, the structural and the magnetic transition were assigned to a simultaneous 2nd order transition.⁵² Therefore, charge compensated $\text{Ba}_{1-x}\text{K}_x(\text{Fe}_{1-y}\text{Co}_y)_2\text{As}_2$ is likely to behave similar in that sense. However, the *linear* coupling between the structural and the magnetic order parameter in the vicinity of the phase transitions in $\text{Ba}_{1-x}\text{K}_x(\text{Fe}_{1-y}\text{Co}_y)_2\text{As}_2$ from Fig. 13 is not compatible with a second order, harmonic magneto-elastic coupling scenario for which a *quadratic* coupling is mandatory by symmetry. Nevertheless, following Refs.^{60,64,65} *bilinear* coupling exists between the nematic and structural order parameter which implies a simultaneous nematic-magnetic and structural transition. Identifying T_N^{onset} as the nematic phase transition temperature would at least give qualitatively a consistent explanation for our experimental findings. This includes our observation, that static magnetism coexists together with superconductivity in a tetragonal structure for $0.15 \leq x/2 \approx y \leq 0.19$.

	δ_S (10^{-3})	B_{hf} (T)	$M(\mu_B, T=0)$
BaFe ₂ As ₂ :	3.6 ³³	5.4 ³³	
EuFe ₂ As ₂ :	5.1 ^{66,67}	8.0 ⁶⁸	
SrFe ₂ As ₂ :	5.7 ⁶⁹	8.8 ^{69,70}	
CaFe ₂ As ₂ :	5.1 ⁷¹	8.2 ⁷²	
	6.2 ⁶⁷	8.5 ⁶⁸	
	6.6 ⁷³	10.2 ⁷⁴	
	7.0 ⁷⁵	10.2 ⁷⁶	
used	6.2 \pm 1	9.2 \pm 1	
LaOFeAs:	2.6 ⁷⁷	4.9 ⁷⁸	
CeOFeAs:	2.6 ⁷⁹	5.4 ^{79,80}	
NdOFeAs:	2.4 ⁸¹	5.3 ⁸⁰	
SmOFeAs:	2.7 ⁷⁹	5.2 ⁷⁹	
PrOFeAs:	1.9 ⁴⁴	5.0 ^{44,80}	
	2.8 ⁴⁴		
used	2.3 \pm 0.5	5.0	
Ba(Fe _{1-x} Ru _x) ₂ As ₂			
$x_{\text{Ru}} = 0.073$:	1.1 ^{52,54}		0.3 ⁵²
$x_{\text{Ru}} = 0.205$:	2.6 ⁵²		0.6 ⁵²

TABLE II: Low temperature values and references for the orthorhombic splitting and the ordered magnetic moment for selected 122 and 1111 iron-pnictides shown in Fig. 13

V. SUMMARY

The experimental results on charge compensated Ba_{1-x}K_x(Fe_{1-y}Co_y)₂As₂ with $x/2 \approx y$ are summarized in a phase diagram in Fig. 14 (right panel) in comparison with full phase diagram of Ba_{1-x}K_x(Fe_{1-y}Co_y)₂As₂ for $x/2 \leq 0.25$ and $y \leq 0.25$ (left panel). In the charge compensated state, the reported²⁴ transition from an antiferromagnetic metal ($x/2 \approx y \leq 0.10$) with an orthorhombic structure to a tetragonal, non-magnetic ground state ($x/2 \approx y \geq 0.25$) was confirmed. However, local probe techniques evidences that static magnetic order extends to a higher substitution level ($x/2 \approx y \leq 0.19$) than reported previously ($x/2 \approx y \leq 0.10$).²⁴ Moreover, magnetism coexists in a tetragonal structure together with superconductivity for $0.15 \leq x/2 \approx y \leq 0.19$.

We have discussed the electronic phase diagram of

charge compensated Ba_{1-x}K_x(Fe_{1-y}Co_y)₂As₂ within an empirical model which indirectly includes the local defects in an effective Stoner-like picture. The shape of the superconducting dome can be explained by the introduction of disorder due to non-magnetic impurities (n_{imp}) to a system with a constant charge carrier density.⁵⁷ A comparison of the T_c - n_{imp} phase diagrams suggests that the quasi-particle scattering in charge compensated Ba_{1-x}K_x(Fe_{1-y}Co_y)₂As₂ is dominantly due to intraband processes. The measured temperature dependence of the magnetic penetration depth for the sample with $x/2 \approx y = 0.19$ suggests a nodeless symmetry for the superconducting order parameter in accordance with the predicted s^{\pm} pairing symmetry. Superconductivity in effectively carrier-free Ba_{1-x}K_x(Fe_{1-y}Co_y)₂As₂ is weaker ($T_{c,\text{max}} \sim 15$ K) compared to carrier doped Ba_{1-x}K_xFe₂As₂ (38 K) and Ba(Fe_{1-x}Co_x)₂As₂ (23 K) since it is allways competing with magnetism.

Furthermore, our results prove that magnetism is present throughout the whole superconducting dome. From this finding in addition with the temperature independent, linear relationship between the magnetic and structural order parameter defined as the normalized orthorhombic splitting δ_s and the weighted hyperfine field B_{hf} (see Fig.13), we conclude that for effectively charge compensated Ba_{1-x}K_x(Fe_{1-y}Co_y)₂As₂, the orthorhombic lattice distortion and the onset of superconductivity is controlled by the magnetic, potentially nematic-magnetic, instability.

Acknowledgments

This work was financially supported by the German Research Foundation (DFG) within the priority program SPP 1458 projects JO257/6-1 and KL1086/10-1. Additional DFG support within the framework of the Research Training Group GRK 1621 is acknowledged. Part of this work was performed at the Swiss Muon Source (Villigen, Switzerland). T.G. thanks Johannes Spehling and Rajib Sarkar for valuable discussions.

¹ Y. Kamihara, T. Watanabe, M. Hirano, and H. Hosono, Journal of the American Chemical Society **130**, 3296 (2008), URL <http://pubs.acs.org/doi/abs/10.1021/ja800073m>.

² M. Rotter, M. Tegel, and D. Johrendt, Phys. Rev. Lett. **101**, 107006 (2008), URL <http://link.aps.org/doi/10.1103/PhysRevLett.101.107006>.

³ A. Leithe-Jasper, W. Schnelle, C. Geibel, and H. Rosner, Phys. Rev. Lett. **101**, 207004 (2008), URL <http://link.aps.org/doi/10.1103/PhysRevLett.101.207004>.

⁴ F. Ronning, T. Klimczuk, E. D. Bauer, H. Volz, and J. D. Thompson, Journal of Physics: Condensed Matter **20**, 322201 (2008), URL <http://stacks.iop.org/0953-8984/20/i=32/a=322201>.

⁵ P. L. Alireza, Y. T. C. Ko, J. Gillett, C. M. Petrone, J. M. Cole, G. G. Lonzarich, and S. E. Sebastian, Journal of Physics: Condensed Matter **21**, 012208 (2009), URL <http://stacks.iop.org/0953-8984/21/i=1/a=012208>.

⁶ J. Paglione and R. L. Greene, Nature Physics **6**, 645 (2010), ISSN 1745-2473, URL <http://dx.doi.org/10.1038/nphys1759>.

⁷ P. Canfield and S. Bud'ko, Annu. Rev. Condens. Matter Phys. **1**, 27 (2010), URL <http://www.annualreviews.org/doi/abs/10.1146/annurev-conmatphys-070909-104041>.

⁸ A. S. Sefat, R. Jin, M. A. McGuire, B. C. Sales, D. J. Singh,

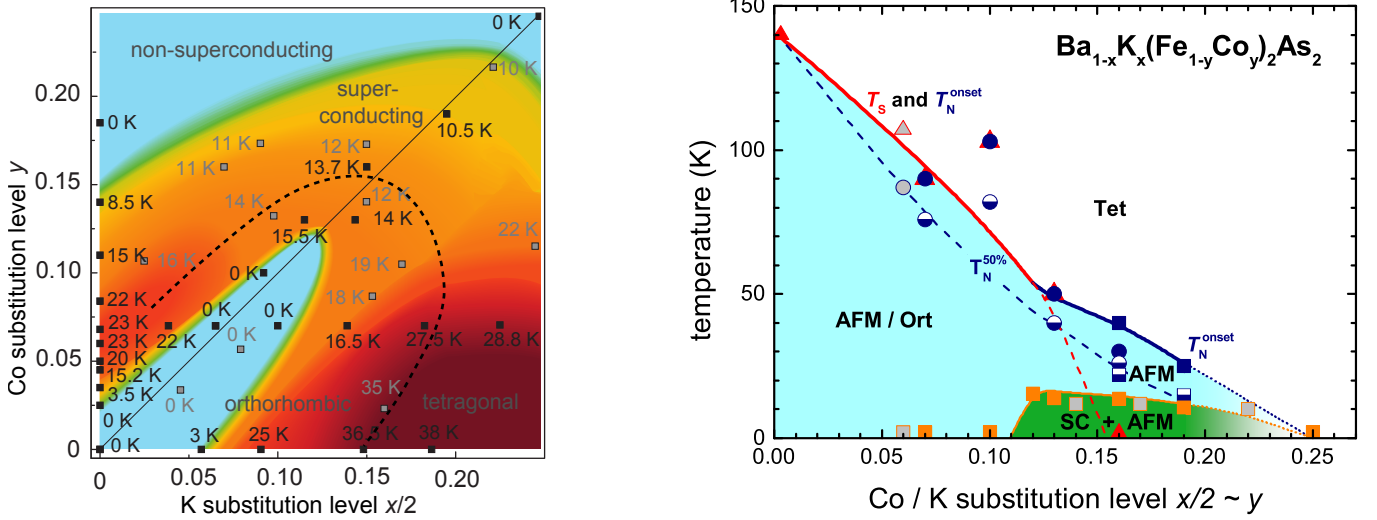


FIG. 14: Left panel: Full phase diagram of $\text{Ba}_{1-x}\text{K}_x(\text{Fe}_{1-y}\text{Co}_y)_2\text{As}_2$ for $x/2$ and $y \leq 0.25$: Black squares refer to the corresponding superconducting transition temperatures for $\text{Ba}_{1-x}\text{K}_x\text{Fe}_2\text{As}_2$,¹³ $\text{Ba}(\text{Fe}_{1-x}\text{Co}_x)_2\text{As}_2$ ⁸² and $\text{Ba}_{1-x}\text{K}_x(\text{Fe}_{1-y}\text{Co}_y)_2\text{As}_2$ from this work. Grey squares for $\text{Ba}_{1-x}\text{K}_x(\text{Fe}_{1-y}\text{Co}_y)_2\text{As}_2$ are taken from Ref.²⁴ A non-superconducting groundstate is depicted in blue and superconductivity is shown color-coded from yellow (for $T_c \approx 10$ K) to dark red ($T_c \approx 40$ K). Dashed line: Tentative border for the existence of the orthorhombic phase. Right panel: Phase diagram of charge compensated $\text{Ba}_{1-x}\text{K}_x(\text{Fe}_{1-y}\text{Co}_y)_2\text{As}_2$. Data points refer to results from x-ray diffraction (red triangles), Mössbauer spectroscopy (blue circles) and muon spin relaxation (blue squares); T^{onset} in full symbols, $T^{50\%}$ in half symbols. Data points for the corresponding transition temperatures from Ref.²⁴ were added in grey.

- and D. Mandrus, Phys. Rev. Lett. **101**, 117004 (2008), URL <http://link.aps.org/doi/10.1103/PhysRevLett.101.117004>.
- ⁹ N. Ni, A. Thaler, A. Kracher, J. Q. Yan, S. L. Bud'ko, and P. C. Canfield, Phys. Rev. B **80**, 024511 (2009), URL <http://link.aps.org/doi/10.1103/PhysRevB.80.024511>.
- ¹⁰ N. Ni, A. Thaler, J. Q. Yan, A. Kracher, E. Colambier, S. L. Bud'ko, P. C. Canfield, and S. T. Hannahs, Phys. Rev. B **82**, 024519 (2010), URL <http://link.aps.org/doi/10.1103/PhysRevB.82.024519>.
- ¹¹ F. Han, X. Zhu, P. Cheng, G. Mu, Y. Jia, L. Fang, Y. Wang, H. Luo, B. Zeng, B. Shen, et al., Phys. Rev. B **80**, 024506 (2009), URL <http://link.aps.org/doi/10.1103/PhysRevB.80.024506>.
- ¹² S. R. Saha, T. Drye, K. Kirshenbaum, N. P. Butch, P. Y. Zavalij, and J. Paglione, Journal of Physics: Condensed Matter **22**, 072204 (2010), URL <http://stacks.iop.org/0953-8984/22/i=7/a=072204>.
- ¹³ M. Rotter, M. Pangerl, M. Tegel, and D. Johrendt, Angewandte Chemie International Edition **47**, 7949 (2008), ISSN 1521-3773, URL <http://dx.doi.org/10.1002/anie.200803641>.
- ¹⁴ D. K. Pratt, W. Tian, A. Kreyssig, J. L. Zarestky, S. Nandi, N. Ni, S. L. Bud'ko, P. C. Canfield, A. I. Goldman, and R. J. McQueeney, Phys. Rev. Lett. **103**, 087001 (2009), URL <http://link.aps.org/doi/10.1103/PhysRevLett.103.087001>.
- ¹⁵ E. Wiesenmayer, H. Luetkens, G. Pascua, R. Khasanov, A. Amato, H. Potts, B. Banusch, H.-H. Klauss, and D. Johrendt, Phys. Rev. Lett. **107**, 237001 (2011), URL <http://link.aps.org/doi/10.1103/PhysRevLett.107.237001>.
- ¹⁶ Y. Liu, D. Sun, J. Park, and C. Lin, Physica C: Superconductivity **470**, Supplement 1, S513 (2010), ISSN 0921-4534, URL <http://www.sciencedirect.com/science/article/pii/S0921453409007369>.
- ¹⁷ A. S. Sefat, D. J. Singh, L. H. VanBebber, Y. Mozharivskyj, M. A. McGuire, R. Jin, B. C. Sales, V. Keppens, and D. Mandrus, Phys. Rev. B **79**, 224524 (2009), URL <http://link.aps.org/doi/10.1103/PhysRevB.79.224524>.
- ¹⁸ H. Wadati, I. Elfimov, and G. A. Sawatzky, Phys. Rev. Lett. **105**, 157004 (2010), URL <http://link.aps.org/doi/10.1103/PhysRevLett.105.157004>.
- ¹⁹ T. Berlijn, C.-H. Lin, W. Garber, and W. Ku, Phys. Rev. Lett. **108**, 207003 (2012), URL <http://link.aps.org/doi/10.1103/PhysRevLett.108.207003>.
- ²⁰ S. Ideta, T. Yoshida, I. Nishi, A. Fujimori, Y. Kotani, K. Ono, Y. Nakashima, S. Yamaichi, T. Sasagawa, M. Nakajima, et al., Phys. Rev. Lett. **110**, 107007 (2013), URL <http://link.aps.org/doi/10.1103/PhysRevLett.110.107007>.
- ²¹ R. Kraus, V. Bisogni, L. Harnagea, S. Aswartham, S. Wurmehl, G. Levy, I. S. Elfimov, B. Büchner, G. A. Sawatzky, and J. Geck, Phys. Rev. B **87**, 134516 (2013), URL <http://link.aps.org/doi/10.1103/PhysRevB.87.134516>.
- ²² S. Sharma, A. Bharathi, S. Chandra, V. R. Reddy, S. Paulraj, A. T. Satya, V. S. Sastry, A. Gupta, and C. S. Sundar, Phys. Rev. B **81**, 174512 (2010), URL <http://link.aps.org/doi/10.1103/PhysRevB.81.174512>.
- ²³ S. Jiang, H. Xing, G. Xuan, C. Wang, Z. Ren, C. Feng, J. Dai, Z. Xu, and G. Cao, Journal of Physics: Condensed Matter **21**, 382203 (2009), URL <http://stacks.iop.org/0953-8984/21/i=38/a=382203>.
- ²⁴ S. Suzuki, K. Ohgushi, Y. Kiuchi, and Y. Ueda, Phys. Rev.

- B **82**, 184510 (2010), URL <http://link.aps.org/doi/10.1103/PhysRevB.82.184510>.
- ²⁵ V. Zinth, T. Dellmann, H.-H. Klauss, and D. Johrendt, *Angewandte Chemie International Edition* **50**, 7919 (2011), ISSN 1521-3773, URL <http://dx.doi.org/10.1002/anie.201102866>.
 - ²⁶ M. Neupane, P. Richard, Y.-M. Xu, K. Nakayama, T. Sato, T. Takahashi, A. V. Federov, G. Xu, X. Dai, Z. Fang, et al., *Phys. Rev. B* **83**, 094522 (2011), URL <http://link.aps.org/doi/10.1103/PhysRevB.83.094522>.
 - ²⁷ A. Suter and B. Wojek, *Physics Procedia* **30**, 69 (2012), ISSN 1875-3892, 12th International Conference on Muon Spin Rotation, Relaxation and Resonance (MuSR2011), URL <http://www.sciencedirect.com/science/article/pii/S187538921201228X>.
 - ²⁸ K. Koepnik and H. Eschrig, *Phys. Rev. B* **59**, 1743 (1999), URL <http://link.aps.org/doi/10.1103/PhysRevB.59.1743>.
 - ²⁹ I. Opahle, K. Koepnik, and H. Eschrig, *Phys. Rev. B* **60**, 14035 (1999), URL <http://link.aps.org/doi/10.1103/PhysRevB.60.14035>.
 - ³⁰ J. P. Perdew and Y. Wang, *Phys. Rev. B* **45**, 13244 (1992), URL <http://link.aps.org/doi/10.1103/PhysRevB.45.13244>.
 - ³¹ D. Kasinathan, M. Wagner, K. Koepnik, R. Cardoso-Gil, Y. Grin, and H. Rosner, *Phys. Rev. B* **85**, 035207 (2012), URL <http://link.aps.org/doi/10.1103/PhysRevB.85.035207>.
 - ³² V. Zinth, Ph.D. thesis, Ludwig-Maximilians-Universität München (2012), URL <http://nbn-resolving.de/urn:nbn:de:bvb:19-144965>.
 - ³³ M. Rotter, M. Tegel, I. Schellenberg, F. M. Schappacher, R. Pöttgen, J. Deisenhofer, A. Günther, F. Schrettle, A. Loidl, and D. Johrendt, *New J. Phys.* **11**, 025014 (2009), URL <http://stacks.iop.org/1367-2630/11/i=2/a=025014>.
 - ³⁴ D. G. Rancourt and J. Y. Ping, *Nuclear Instruments and Methods in Physics Research Section B: Beam Interactions with Materials and Atoms* **58**, 85 (1991), ISSN 0168-583X, URL <http://www.sciencedirect.com/science/article/pii/0168583X91956813>.
 - ³⁵ M. Rotter, M. Tegel, D. Johrendt, I. Schellenberg, W. Hermes, and R. Pöttgen, *Phys. Rev. B* **78**, 020503 (2008), URL <http://link.aps.org/doi/10.1103/PhysRevB.78.020503>.
 - ³⁶ H. Luetkens, H.-H. Klauss, M. Kraken, F.-J. Litterst, T. Dellmann, R. Klingeler, C. Hess, R. Khasanov, A. Amato, C. Baines, et al., *Nature Materials* **8**, 305 (2009), ISSN 1476-1122, URL <http://www.nature.com/nmat/journal/v8/n4/full/nmat2397.html>.
 - ³⁷ P. Marsik, K. W. Kim, A. Dubroka, M. Rössle, V. K. Malik, L. Schulz, C. N. Wang, C. Niedermayer, A. J. Drew, M. Willis, et al., *Phys. Rev. Lett.* **105**, 057001 (2010), URL <http://link.aps.org/doi/10.1103/PhysRevLett.105.057001>.
 - ³⁸ C. Bernhard, C. N. Wang, L. Nuccio, L. Schulz, O. Zakharko, J. Larsen, C. Aristizabal, M. Willis, A. J. Drew, G. D. Varma, et al., *Phys. Rev. B* **86**, 184509 (2012), URL <http://link.aps.org/doi/10.1103/PhysRevB.86.184509>.
 - ³⁹ H. Maeter, G. Pascua, H. Luetkens, J. Knolle, S. Aswartham, S. Wurmehl, G. Behr, B. Büchner, Z. Shermadini, K. Sedlak, et al., *ArXiv e-prints* (2012), 1210.6881, URL <http://arxiv.org/abs/1210.6881>.
 - ⁴⁰ R. S. Hayano, Y. J. Uemura, J. Imazato, N. Nishida, T. Yamazaki, and R. Kubo, *Phys. Rev. B* **20**, 850 (1979), URL <http://link.aps.org/doi/10.1103/PhysRevB.20.850>.
 - ⁴¹ E. H. Brandt, *Phys. Rev. B* **37**, 2349 (1988), URL <http://link.aps.org/doi/10.1103/PhysRevB.37.2349>.
 - ⁴² J. E. Sonier, J. H. Brewer, and R. F. Kiefl, *Rev. Mod. Phys.* **72**, 769 (2000), URL <http://link.aps.org/doi/10.1103/RevModPhys.72.769>.
 - ⁴³ J. E. Sonier, W. Huang, C. V. Kaiser, C. Cochran, V. Pacradouni, S. A. Sabok-Sayr, M. D. Lumsden, B. C. Sales, M. A. McGuire, A. S. Sefat, et al., *Phys. Rev. Lett.* **106**, 127002 (2011), URL <http://link.aps.org/doi/10.1103/PhysRevLett.106.127002>.
 - ⁴⁴ H. Luetkens (private communication).
 - ⁴⁵ K. Yosida, *Phys. Rev.* **110**, 769 (1958), URL <http://link.aps.org/doi/10.1103/PhysRev.110.769>.
 - ⁴⁶ R. Khasanov, A. Maisuradze, H. Maeter, A. Kwadrin, H. Luetkens, A. Amato, W. Schnelle, H. Rosner, A. Leithe-Jasper, and H.-H. Klauss, *Phys. Rev. Lett.* **103**, 067010 (2009), URL <http://link.aps.org/doi/10.1103/PhysRevLett.103.067010>.
 - ⁴⁷ T. J. Williams, A. A. Aczel, E. Baggio-Saitovitch, S. L. Bud'ko, P. C. Canfield, J. P. Carlo, T. Goko, H. Kageyama, A. Kitada, J. Munevar, et al., *Phys. Rev. B* **82**, 094512 (2010), URL <http://link.aps.org/doi/10.1103/PhysRevB.82.094512>.
 - ⁴⁸ H. Maeter, Ph.D. thesis, Technische Universität Dresden (2012), URL http://slubdd.de/katalog?libero_mab215837718.
 - ⁴⁹ D. V. Evtushinsky, D. S. Inosov, V. B. Zabolotnyy, M. S. Viazovska, R. Khasanov, A. Amato, H.-H. Klauss, H. Luetkens, C. Niedermayer, G. L. Sun, et al., *New Journal of Physics* **11**, 055069 (2009), URL <http://stacks.iop.org/1367-2630/11/i=5/a=055069>.
 - ⁵⁰ Y. Laplace, J. Bobroff, V. Brouet, G. Collin, F. Rullier-Albenque, D. Colson, and A. Forget, *Phys. Rev. B* **86**, 020510 (2012), URL <http://link.aps.org/doi/10.1103/PhysRevB.86.020510>.
 - ⁵¹ A. Thaler, N. Ni, A. Kracher, J. Q. Yan, S. L. Bud'ko, and P. C. Canfield, *Phys. Rev. B* **82**, 014534 (2010), URL <http://link.aps.org/doi/10.1103/PhysRevB.82.014534>.
 - ⁵² M. G. Kim, D. K. Pratt, G. E. Rustan, W. Tian, J. L. Zarestky, A. Thaler, S. L. Bud'ko, P. C. Canfield, R. J. McQueeney, A. Kreyssig, et al., *Phys. Rev. B* **83**, 054514 (2011), URL <http://link.aps.org/doi/10.1103/PhysRevB.83.054514>.
 - ⁵³ R. S. Dhaka, C. Liu, R. M. Fernandes, R. Jiang, C. P. Strehlow, T. Kondo, A. Thaler, J. Schmalian, S. L. Bud'ko, P. C. Canfield, et al., *Phys. Rev. Lett.* **107**, 267002 (2011), URL <http://link.aps.org/doi/10.1103/PhysRevLett.107.267002>.
 - ⁵⁴ M. G. Kim, J. Soh, J. Lang, M. P. M. Dean, A. Thaler, S. L. Bud'ko, P. C. Canfield, E. Bourret-Courchesne, A. Kreyssig, A. I. Goldman, et al., *Phys. Rev. B* **88**, 014424 (2013), URL <http://link.aps.org/doi/10.1103/PhysRevB.88.014424>.
 - ⁵⁵ F. Ning, K. Ahilan, T. Imai, A. S. Sefat, R. Jin, M. A. McGuire, B. C. Sales, and D. Mandrus, *Journal of the Physical Society of Japan* **77**, 103705 (2008), URL <http://jpsj.ipap.jp/link?JPSJ/77/103705/>.
 - ⁵⁶ D. J. Singh, *Phys. Rev. B* **79**, 174520 (2009), URL <http://link.aps.org/doi/10.1103/PhysRevB.79.174520>.
 - ⁵⁷ M. Vavilov and A. Chubukov, *Phys. Rev. B* **84**, 214521 (2011), URL <http://link.aps.org/doi/10.1103/>

- PhysRevB. **84**.214521.
- ⁵⁸ R. M. Fernandes, D. K. Pratt, W. Tian, J. Zarestky, A. Kreyssig, S. Nandi, M. G. Kim, A. Thaler, N. Ni, P. C. Canfield, et al., Phys. Rev. B **81**, 140501 (2010), URL <http://link.aps.org/doi/10.1103/PhysRevB.81.140501>.
 - ⁵⁹ P. C. Canfield, S. L. Bud'ko, N. Ni, J. Q. Yan, and A. Kracher, Phys. Rev. B **80**, 060501 (2009), URL <http://link.aps.org/doi/10.1103/PhysRevB.80.060501>.
 - ⁶⁰ M. G. Kim, R. M. Fernandes, A. Kreyssig, J. W. Kim, A. Thaler, S. L. Bud'ko, P. C. Canfield, R. J. McQueeney, J. Schmalian, and A. I. Goldman, Phys. Rev. B **83**, 134522 (2011), URL <http://link.aps.org/doi/10.1103/PhysRevB.83.134522>.
 - ⁶¹ H. Maeter, H. Luetkens, Y. G. Pashkevich, A. Kwadrin, R. Khasanov, A. Amato, A. A. Gusev, K. V. Lamonova, D. A. Chervinskii, R. Klingeler, et al., Phys. Rev. B **80**, 094524 (2009), URL <http://link.aps.org/doi/10.1103/PhysRevB.80.094524>.
 - ⁶² S. D. Wilson, C. R. Rotundu, Z. Yamani, P. N. Valdivia, B. Freelon, E. Bourret-Courchesne, and R. J. Birgeneau, Phys. Rev. B **81**, 014501 (2010), URL <http://link.aps.org/doi/10.1103/PhysRevB.81.014501>.
 - ⁶³ A. Cano, M. Civelli, I. Eremin, and I. Paul, Phys. Rev. B **82**, 020408 (2010), URL <http://link.aps.org/doi/10.1103/PhysRevB.82.020408>.
 - ⁶⁴ R. M. Fernandes, L. H. VanBebber, S. Bhattacharya, P. Chandra, V. Keppens, D. Mandrus, M. A. McGuire, B. C. Sales, A. S. Sefat, and J. Schmalian, Phys. Rev. Lett. **105**, 157003 (2010), URL <http://link.aps.org/doi/10.1103/PhysRevLett.105.157003>.
 - ⁶⁵ R. M. Fernandes, A. V. Chubukov, J. Knolle, I. Eremin, and J. Schmalian, Phys. Rev. B **85**, 024534 (2012), URL <http://link.aps.org/doi/10.1103/PhysRevB.85.024534>.
 - ⁶⁶ M. Tegel, M. Rotter, V. Weiß, F. M. Schappacher, R. Pöettgen, and D. Johrendt, Journal of Physics: Condensed Matter **20**, 452201 (2008), URL <http://stacks.iop.org/0953-8984/20/i=45/a=452201>.
 - ⁶⁷ S. K. Mishra, R. Mittal, P. S. R. Krishna, P. U. Sastry, S. L. Chaplot, S. Matsuiishi, and H. Hosono, ArXiv e-prints (2013), 1304.0595.
 - ⁶⁸ A. Błachowski, K. Ruebenbauer, J. Żukrowski, K. Rogacki, Z. Bukowski, and J. Karpinski, Phys. Rev. B **83**, 134410 (2011), URL <http://link.aps.org/doi/10.1103/PhysRevB.83.134410>.
 - ⁶⁹ A. Jesche, N. Caroca-Canales, H. Rosner, H. Borrmann, A. Ormeci, D. Kasinathan, H. H. Klauss, H. Luetkens, R. Khasanov, A. Amato, et al., Phys. Rev. B **78**, 180504 (2008), URL <http://link.aps.org/doi/10.1103/PhysRevB.78.180504>.
 - ⁷⁰ Z. Li, X. Ma, H. Pang, and F. Li, Hyperfine Interactions **207**, 41 (2012), 1110.3550, URL <http://adsabs.harvard.edu/abs/2012HyInt..207...41L>.
 - ⁷¹ A. I. Goldman, D. N. Argyriou, B. Ouladdiaf, T. Chatterji, A. Kreyssig, S. Nandi, N. Ni, S. L. Budko, P. C. Canfield, and R. J. McQueeney, Phys. Rev. B **78**, 100506 (2008), URL <http://link.aps.org/doi/10.1103/PhysRevB.78.100506>.
 - ⁷² Z. Li, X. Ma, H. Pang, and F. Li, Journal of Physics: Condensed Matter **23**, 255701 (2011), URL <http://stacks.iop.org/0953-8984/23/i=25/a=255701>.
 - ⁷³ N. Ni, S. Nandi, A. Kreyssig, A. I. Goldman, E. D. Mun, S. L. Bud'ko, and P. C. Canfield, Phys. Rev. B **78**, 014523 (2008), URL <http://link.aps.org/doi/10.1103/PhysRevB.78.014523>.
 - ⁷⁴ M. Alzamora, J. Munevar, E. Baggio-Saitovitch, S. L. Budko, N. Ni, P. C. Canfield, and D. R. Sanchez, Journal of Physics: Condensed Matter **23**, 145701 (2011), URL <http://stacks.iop.org/0953-8984/23/i=14/a=145701>.
 - ⁷⁵ A. I. Goldman, D. N. Argyriou, B. Ouladdiaf, T. Chatterji, A. Kreyssig, S. Nandi, N. Ni, S. L. Bud'ko, P. C. Canfield, and R. J. McQueeney, Phys. Rev. B **78**, 100506 (2008), URL <http://link.aps.org/doi/10.1103/PhysRevB.78.100506>.
 - ⁷⁶ N. Kumar, R. Nagalakshmi, R. Kulkarni, P. L. Paulose, A. K. Nigam, S. K. Dhar, and A. Thamizhavel, Phys. Rev. B **79**, 012504 (2009), URL <http://link.aps.org/doi/10.1103/PhysRevB.79.012504>.
 - ⁷⁷ T. Nomura, S. W. Kim, Y. Kamihara, M. Hirano, P. V. Sushko, K. Kato, M. Takata, A. L. Shluger, and H. Hosono, Superconductor Science and Technology **21**, 125028 (2008), URL <http://stacks.iop.org/0953-2048/21/i=12/a=125028>.
 - ⁷⁸ H.-H. Klauss, H. Luetkens, R. Klingeler, C. Hess, F. J. Litterst, M. Kraken, M. M. Korshunov, I. Eremin, S.-L. Drechsler, R. Khasanov, et al., Phys. Rev. Lett. **101**, 077005 (2008), URL <http://link.aps.org/doi/10.1103/PhysRevLett.101.077005>.
 - ⁷⁹ H. Maeter, J. E. Hamann Borrero, T. Goltz, J. Spehling, A. Kwadrin, A. Kondrat, L. Veyrat, G. Lang, H.-J. Grafe, C. Hess, et al., ArXiv e-prints (2012), 1210.6959.
 - ⁸⁰ M. A. McGuire, R. P. Hermann, A. S. Sefat, B. C. Sales, R. Jin, D. Mandrus, F. Grandjean, and G. J. Long, New Journal of Physics **11**, 025011 (2009), URL <http://stacks.iop.org/1367-2630/11/i=2/a=025011>.
 - ⁸¹ W. Tian, W. Ratchiff, M. G. Kim, J.-Q. Yan, P. A. Kienzle, Q. Huang, B. Jensen, K. W. Dennis, R. W. McCallum, T. A. Lograsso, et al., Phys. Rev. B **82**, 060514 (2010), URL <http://link.aps.org/doi/10.1103/PhysRevB.82.060514>.
 - ⁸² N. Ni, M. E. Tillman, J.-Q. Yan, A. Kracher, S. T. Hannahs, S. L. Bud'ko, and P. C. Canfield, Phys. Rev. B **78**, 214515 (2008), URL <http://link.aps.org/doi/10.1103/PhysRevB.78.214515>.
 - ⁸³ For version details see <http://www.fplo.de>
 - ⁸⁴ $\sigma_{\text{hf}} = 0.5$ T was chosen, so that $2\sigma_{\text{hf}} = \Gamma/4$. This value corresponds to the experimental resolution limit due to the $^{57}\text{Co}/\text{Rh}$ sources line width (FWHM) of $\Gamma = 0.27$ mm/s.
 - ⁸⁵ Nuclear and vortex lattice contributions to the measured relaxation rate were separated in the following way: Since the nuclear contribution is a convolution of a lorentzian and gaussian relaxation rate (see Eq. (1)), the two components were subtracted quadratically for the gaussian and linearly for the lorentzian in the frequency (field) domain: $\sigma_{\text{SC}}(T) = \sqrt{\sigma^2(T) - \sigma_{\text{nucl}}^2} - \lambda_{\text{nucl}}$. The values for $\sigma_{\text{nucl}} = 0.14 \mu\text{s}^{-1}$ and $\lambda_{\text{nucl}} = 0.05 \mu\text{s}^{-1}$ are obtained from the zero field measurements.